The epigenetic response of mouse brown adipose tissue to cold stress: histone proteoform, DNA methylation, and RNA expression

Bethany C. Taylor[1], Loic H. Steinthal[2], Michelle Dias[3], Hari K. Yalamanchili[2,3], Scott A. Ochsner[4], Gladys E. Zapata[2], Nitesh R. Mehta[2], Neil J. McKenna[4], Nicolas L. Young[1,4,5,6†], Alli M. Nuotio-Antar[2,†]

[1] Verna & Marrs McLean Department of Biochemistry & Molecular Pharmacology, Baylor College of Medicine, Houston, TX

[2] Children's Nutrition Research Center, Baylor College of Medicine, Houston, TX

[3] Jan and Dan Duncan Neurological Research Institute, Baylor College of Medicine, Houston, TX

[4] Department of Molecular and Cellular Biology, Baylor College of Medicine, Houston, TX

[5] Center for Precision Environmental Health, Baylor College of Medicine, Houston, TX

[6] Dan L. Duncan Comprehensive Cancer Center, Baylor College of Medicine, Houston, TX

[†] Correspondence to: antar@bcm.edu, nicolas.young@bcm.edu

Mouse BAT Cold Stress

Abbreviations

ACN Acetonitrile

AEBSF 4-benzenesulfonyl fluoride hydrochloride

AGC Automatic gain control

ANOVA One-way analysis of variance

BAT Brown adipose tissue

C3 3 carbon chain

ChIP-Seq Chromatin immunoprecipitation sequencing

DEG Differentially expressed genes

DMP Differentially methylated promoters

DNA Deoxyribonucleic acid

DNMT1 DNA methyltransferase 1

DNMT3B DNA methyltransferase 3B

DNL Day night average sound level

DTT Dithiothreitol

ETD Electron transfer dissociation

EZH2 Enhancer of zeste homolog 2

FA Formic acid

FC Fold change

FCOR FOXO1-corepressor

FDR False discovery rate

FOXO1 Forkhead Box O1

G9a/GLP (EHMT2/EHMT1) Euchromatic histone-lysine N-methyltransferase 2/ Euchromatic histone-lysine N-methyltransferase 1

GluC Staphylococcus aureus Protease V8

HCT High confidence transcriptional target

HDAC3 Histone deacetylase 3

HPLC High-performance liquid chromatography

K Lysine

Kdm2b Lysine (K)-specific demethylase 2B

Kdm3a Lysine demethylase 3A

Kdm5b Lysine-specific demethylase 5B

Kdm5c Lysine demethylase 5C

Kdm8 (JMJD5) Lysine demethylase 8

LC-MS/MS Liquid chromatography tandem mass spectrometry

MACS2 Model-based analysis of ChIP-seq

MS Mass spectrometry

MS2 Tandem mass spectrometry or mass spectrum

mzXML File format, eXtensible markup language

NAD+ Nicotinamide adenine dinucleotide

NIB Nuclei isolation buffer

NP-40 Nonyl phenoxypolyethoxylethanol

NST Nonshivering thermogenesis

OR Odds ratio

PRC2 Polycomb repressive complex 2

PTM Post-translational modification

RNA-Seq RNA sequencing

RRBS Reduced representation bisulfite sequencing

RT Room temperature

SAM S-adenosyl methionine

SIRT1 Sirtuin-1

SC Severe cold

SEM Standard error of the mean

Setd7 Histone-lysine N-methyltransferase SETD7

SIRT1 Sirtuin-1

SMYD3 SET and MYN-domain containing 3

SRA Sequence Read Archive

SUV39H1 Histone-lysine N-methyltransferase SUV39H1

SUV39H2 Histone-lysine N-methyltransferase SUV39H2

TFA Trifluoroacetic acid

TN Thermoneutral

UCP1 Uncoupling protein 1

Mouse BAT Cold Stress

WAT White adipose tissue

Abstract

Regulation of the thermogenic response by brown adipose tissue (BAT) is an important component of energy homeostasis with implications for the treatment of obesity and diabetes. Motivated to understand how BAT function is regulated epigenetically, we reanalyzed publicly available RNA-seq data and uncovered many nodes representing epigenetic modifiers that are altered in BAT in response to chronic thermogenic activation. Thus, we hypothesized that chronic thermogenic activation broadly alters epigenetic modifications of DNA and histones in BAT. To test our hypothesis, wildtype male C57BL/6J mice were housed under chronic conditions of thermoneutral temperature (TN, 28.8°C), mild cold/room temperature (RT, 22°C), or severe cold (SC, 8°C). BAT and reference tissue liver were subsequently dissected from each mouse. Reduced representation bisulfite sequencing (RRBS) reveals decreased methylation of promoters and intragenic regions in BAT genomic DNA in response to varying degrees of chronic cold exposure. Integration of our RRBS and the RNA-Seq dataset suggests a role for epigenetic modification of DNA in gene regulation in response to cold. To analyze histone modifications in BAT, we develop a robust method for the isolation of histones and report the first quantitation of histone H3.2 and H4 proteoforms. We initially observe that BAT and liver exhibit different histone proteoforms. Next, we report housing temperature-dependent changes in histone proteoforms in BAT. We observe differences in bivalent proteoforms such as H3{K9me2,K23ac,K36me1}, H3{K9me3,K23ac,K36me1} and H4<K8acK16acK20me3>. Taken together, our results provide novel findings supporting global epigenetic modification in murine BAT in response to varying degrees of chronic cold stimuli and establish a methodology to quantitatively study histones in BAT, allowing

for direct comparisons to decipher mechanistic changes during the thermogenic response.

Introduction

Brown adipose tissue (BAT) is a mitochondria-rich tissue that is essential for maintaining body temperature through nonshivering thermogenesis (NST). BAT is important to many aspects of mammalian energy homeostasis (1). In humans, the percentage of BAT by body weight is greatest in newborn infants and plays an essential role in body temperature regulation in the absence of an adequate shivering response by skeletal muscle (2). Although the percentage of BAT mass by body weight decreases with age in humans, NST contributes significantly to adult resting energy expenditure (3–5). BAT uptake and oxidation of circulating glucose and fatty acid renders the tissue a biologic "sink" for both nutrients. Altered BAT function in adult humans is associated with differences in adiposity, glucose homeostasis, insulin sensitivity, and energy expenditure (3, 6–8). In particular, NST-induced glucose uptake and oxidation by BAT is attenuated in obese and type 2 diabetic patients (9). Therefore, increasing activation of BAT has been suggested as a therapy to counter obesity and type 2 diabetes (3, 10).

Epigenetic regulation of the thermogenic response in BAT remains mostly unexplored but may yield insights into means through which tissue function and consequent beneficial effects on whole-body metabolism may be restored. DNA methyltransferase 1 (DNMT1)-mediated promoter hypermethylation has been shown to repress the expression of pro-myogenic *Myod1* in brown adipocytes, resulting in maintenance of their cell identity (11). BAT-specific deletion of DNA methyltransferase 3B (DNMT3B) increases the expression of genes involved in thermogenesis and mitochondrial biogenesis and blunts high fat diet-induced obesity and insulin resistance in female, but not male, mice (12). Enzymes such as histone deacetylase 3 (HDAC3)

and the nicotinamide adenine dinucleotide (NAD+) dependent deacetylase sirtuin-1 (SIRT1) regulate BAT function (13). HDAC3 primes the expression of uncoupling protein 1 (UCP1) (13). SIRT1 activity has been shown to regulate BAT fatty acid oxidation *in vitro* and expression of thermogenic genes in response to cold *in vivo*, as well as to promote “browning” of white adipocytes (14–17). Thus, while specific enzymes that modulate DNA methylation and histone modifications are required for the proper differentiation and functioning of BAT, information regarding global DNA methylation changes and histone modifications in BAT in response to varying degrees of thermogenic activation is lacking. There is a particular dearth of quantitative data and rigorous comparisons in BAT in response to different thermogenic stimuli and how this differs from other tissues. Histone modifications are particularly less studied in BAT due to a lack of effective methods for the isolation of nuclei from BAT, acid extraction from fatty tissues, and appropriate methods of analysis.

Histone isolation from BAT presents challenges that arise from its unique properties. Brown adipocytes are enriched with multilocular lipid droplets, thus giving them a high lipid content that makes extraction of histones more difficult than for other tissues (18). While we have recently published methods on the efficient extraction of histones from several tissues, additional modifications to our protocols were necessary to enable sufficient yield of histones from BAT (19). Here, we have developed a method to yield sufficient histones for proteomic analysis from murine interscapular BAT depots. Using this novel method, reduced representation bisulfite sequencing (RRBS), and findings from analyses of publicly available RNA-Seq data, we test our hypothesis that the thermogenic response by BAT is associated with multiple epigenetic changes. We

use top- and middle-down mass spectrometry to quantitate discrete post-translational modifications (PTMs) and proteoforms of histones H4 and H3 in BAT and liver from mice housed under thermoneutral or mild or severe chronic cold stress conditions. We thus establish the first quantitative baseline of the BAT histone PTMs and proteoforms. We also compare them to liver and quantitate changes observed during BAT cold adaptation. We additionally observe related changes in gene expression and DNA methylation associated with BAT activation and integrate these findings with observed changes in histone proteoforms and PTMs.

Experimental Procedures

Processing RNA sequencing data

Raw sequencing data was downloaded from Gene Expression Omnibus database under accession number GSE96681, using SRA (Sequence Read Archive) toolkit (20). Sequencing quality and adapter contamination were assessed using FastQC v0.11.9 (21). Overall quality was determined to be satisfactory, and raw reads were aligned to the genome index using STAR v2.7.9a (22). The STAR genome index was created using raw FASTA and annotation files downloaded from the GENCODE portal for mouse genome build GRCm38 release V23. Summary of read and alignment quality were generated using MultiQC v1.12 (23).

Differentially expressed genes: Gene expression values were computed as the number of reads aligned per gene, using STAR—quantMode GeneCounts. Raw counts were normalized, and genes with an average read count < 50 across all samples were excluded from the differential analysis. The analysis for differential gene expression was carried out using DESeq2 (24). A false discovery rate (FDR) cut-off of 0.05 and fold change cut-off of 20% ($-0.263 \leq \log2(FC) \geq +0.263$) were used to identify differentially expressed genes.

Differential splicing analysis: Alternative splicing events were quantified and classified using rMATS (25). Alignment files (BAM) and the GENCODE reference annotation (GTF) for mouse genome build GRCm38 release V23 were used. rMATS classified splicing events into 5 categories: skipped exons, retained introns, mutually exclusive exons, alternative 5’ and 3’ splice sites. An FDR cut-off of 0.05 and an inclusion

level difference cut-off of less than -0.2 or greater than 0.2 were used to screen for statistically significant changes.

Mammalian phenotype ontology analysis

Genes mapping to MPO phenotypes were retrieved from the Mouse Genome Database (26). We retrieved a unique set of nodes (n = 15) mapping to the Mammalian Phenotype Ontology terms “impaired adaptive thermogenesis” (MP:0011049) and “abnormal circadian temperature homeostasis” (MP:0011020) and designated these “thermoregulatory nodes” (27). We then used the hypergeometric test to evaluate the enrichment of thermoregulatory nodes among nodes with the strongest transcriptional footprints among cold challenge-induced gene sets. The universe was set at the total number of unique nodes included in the HCT intersection analysis (n = 691).

Consensus transcriptional regulatory network analysis

High confidence transcriptional target (HCT) intersection analysis of gene sets has been previously described (28–31). Briefly, consensomes are gene lists ranked according to measures of the strength of their regulatory relationship with upstream signaling pathway nodes derived across numerous independent publicly archived transcriptomic or ChIP-Seq datasets (32). To generate mouse ChIP-Seq consensomes, we first retrieved processed gene lists from ChIP-Atlas, in which genes are ranked based on their mean MACS2 peak strength across available archived ChIP-Seq datasets in which a given pathway node is the IP antigen (33). We then mapped the IP antigen to its pathway node category, class, and family, and organized the ranked lists into percentiles to generate

the mouse node ChIP-Seq consensomes (32). Genes in the 95th percentile of a given node consensome were designated high confidence transcriptional targets (HCTs) for that node and used as the input for the HCT intersection analysis using the Bioconductor GeneOverlap analysis package implemented in R. *P*-values were adjusted for multiple testing by using the method of Benjamini & Hochberg to control the false discovery rate as implemented with the p.adjust function in R, to generate *q*-values (34). Evidence for a transcriptional regulatory relationship between a node and a gene set was represented by a larger intersection between the gene set and HCTs for a given node than would be expected by chance after FDR correction ($q < 0.05$).

Mice and dissection

Immediately after weaning at 3 weeks of age, male wildtype C57BL/6J littermates were housed under thermoneutral (TN, 28°C) or mild cold/room temperature (RT, 22ºC) conditions, with an additional cohort of RT-housed mice switched to housing under severe cold (SC, 8ºC) conditions for two weeks, starting at 8 weeks of age. All mice were housed in groups of 2-3 per cage, with a 12h light/12h dark cycle, and were provided adequate bedding and nesting material and unrestricted access to water and a standard chow diet (PicoLab 5V5R) throughout the study. 10-week-old ad lib-fed mice were euthanized between zeitgeber time ZT3-ZT6, and interscapular BAT and liver were dissected and weighed after cardiac perfusion with 20 mL PBS. Tissues were snap-frozen in liquid nitrogen and stored at -80°C immediately after dissection. All animal studies were approved by the Baylor College of Medicine Institutional Animal Care and Usage Committee.

Body Composition

At the end of the study, total fat and lean masses were measured for ad lib-fed mice using an EchoMRI Whole Body Composition Analyzer (Echo Medical Systems) located in the Mouse Metabolic Research Unit at the US Department of Agriculture/Agricultural Research Service (USDA/ARS) Children's Nutrition Research Center (CNRC) at Baylor College of Medicine. For analysis of body composition, nonfasting glucose levels, and body and tissue weights, statistical analysis was performed using GraphPad Prism software (v8.4). One-way analysis of variance (ANOVA) with Tukey posthoc testing was conducted, and data are presented as mean ± the SEM, with $p < 0.05$ considered statistically significant.

Blood glucose measurement

Immediately before sacrifice, mice were retroorbitally bled, and nonfasting glucose was measured using a One Touch Ultra 2 glucose meter and test strips (LifeScan).

Reduced representation bisulfite sequencing

Genomic DNA was extracted from 0.020-0.025g BAT samples obtained from four mice each from TN, RT, and SC groups using a PureLink Genomic DNA Mini Kit (ThermoFisher Scientific) according to manufacturer protocol. Sample libraries were generated from 150 ng genomic DNA and bisulfite conversion was performed using the Ovation RRBS Methyl-Seq System 1-16 with TrueMethyl oxBS kit (Tecan) per manufacturer protocol.

After cleanup, library concentration was measured using a Qubit Fluorometer, and fragment distribution was checked using a 2100 Bioanalyzer high sensitivity chip.

Sequencing at a depth of 50-65 million reads per sample was carried out on an Illumina Nextseq 550 System using a NextSeq 500/550 High Output Kit v2.5 (150 Cycles) (Illumina), per manufacturer protocol for 75 bp paired-end sequencing. Libraries were run on an Illumina Nextseq 550 instrument using the MetSeq Primer 1 (NuGEN) mixed with the Read 1 primer (Illumina) according to the Ovation RRBS Methyl-Seq System 1-16 protocol for the first read and the Read 2 primer (Illumina) for the second read, along with standard Illumina indexing primers. Multiplexed samples were spiked with 10% PhiX Control v3 Library calibration control for run quality monitoring. After the run, FASTQ files were generated using Basespace software (Illumina).

Data processing: Raw read sequencing quality and adapter contamination were assessed using FastQC v0.11.9 (21). Overall quality was determined to be satisfactory, and raw reads were aligned to the bisulfite genome using Bismark v0.23.1 (35). The Bismark bisulfite genome was prepared using the GENCODE raw FASTA file for mouse genome build GRCm38 release 23 and the bowtie2 v2.3.5.1 aligner (36). Alignments were saved as binary format (BAM) files and used to extract methylation calls for CpG, CHG, and CHH contexts using bismark_methylation_extractor. A comprehensive methylation coverage file was also created, detailing the methylation percentage at each base.

Differentially methylated regions: Bismark coverage files were used to generate an object compatible with methylKit v1.20.0 (37), summarizing base-level methylation counts for each sample. Only bases with a minimum read coverage of 10 were retained, and

then normalized using a scaling factor derived from differences between median coverage distributions between samples. Methylation counts were summarized over the promoter and gene body regions, and differentially methylated promoters and genes were identified using an adjusted *p*-value (*q*-value) cutoff of 0.05.

Functional analysis: Functional enrichment analyses were performed on gene lists of interest using WebGestalt (WEB-based GEne SeT AnaLysis Toolkit) with an FDR cutoff of 0.05 (38). Minimum number of genes per category was set to 5. Extracted enrichments were then visualized using GoPlot (39).

Histone isolation

One brown adipose tissue (BAT) and one liver datapoint was achieved for each organism from ~0.1g BAT and ~0.2g liver. BAT samples were homogenized with 1 mL nuclear isolation buffer (NIB) + 0.3% nonyl phenoxypolyethoxylethanol (NP-40) detergent with appropriate epigenetic inhibitors (sodium butyrate, microcystin-LR, 4-benzenesulfonyl fluoride hydrochloride (AEBSF), and dithiothreitol (DTT)) using a Dounce homogenizer. Nuclei isolation was performed as previously described with optimizations of two NIB + NP-40 incubation steps and two NIB-only washes with a centrifuge duration of 10 minutes at 20,000 *x g* (19, 40). Liver samples were homogenized with 1 mL NIB + 1% NP-40 with appropriate epigenetic inhibitors listed above using a Dounce homogenizer. Nuclei isolation was performed as previously described with three NIB-only washes and the centrifuge duration to 10 minutes at 20,000 *x g* (19). Acid extraction was performed as previously described (19). Isolated histones were resuspended in 85 µL 5% acetonitrile,

0.2% trifluoroacetic acid then histone families were separated by offline high-performance liquid chromatography (HPLC) as described in Holt *et al.* (19).

Histone H3 and H4 mass spectrometry method

Histone family offline chromatographic separation: Histone H3 elutes between 42-52 minutes and histone H4 elutes between 34-36.5 minutes with the offline HPLC method used, as previously described (19, 40). H3 variants (H3.1, H3.2, H3.3) and H4 fractions were concentrated to dryness with a vacuum centrifuge concentrator (Savant™ SPD131 SpeedVac, Thermo Scientific, Waltham, MA). For histone H3, a standard curve *µg H3 = (Peak area – 2.6558)/14.221* was used to calculate the mass. Each H3 replicate was resuspended with 10 µL ammonium acetate for digestion with 1:10 mass:mass GluC at 37 °C for one hour. The digestion was quenched by SpeedVac concentration of the sample to dryness.

Preparation of samples for MS and online chromatography: For final dilution, H3 was resuspended to 2 µg/µL using MS buffer A (2% acetonitrile, 0.1% formic acid). For histone H4, dried fractions were diluted using µg H4 = (Peak area – 6.0114)/31.215 to calculate the dilution to 200 ng H4/ µL MS buffer A (2% acetonitrile, 0.1% formic acid). 1 µL diluted histone H3 or H4 was loaded onto a 10 cm, 100 µm inner diameter C3 column (ZORBAX 300SB-C3 300 Å 5 µm) self-packed into fused silica pulled to form a nanoelectrospray emitter. Online HPLC was performed on a Thermo U3000 RSLCnano Pro-flow system. The 70-minute linear gradient using buffer A: 2% acetonitrile, 0.1% formic acid, and B: 98% acetonitrile, 0.1% formic acid is described in **Table 1**. The column eluant was introduced into a Thermo Scientific Orbitrap Fusion Lumos by

nanoelectrospray ionization. Static spray voltages of 2400 V for histone H3 or 1800 V for histone H4 and an ion transfer tube temperature of 320 °C were set for the source.

Mass spectrometry analysis of histone proteoforms: The orbitrap MS1 experiment used a 60k resolution setting in positive mode. An AGC target of 5.0e5 with 200 ms maximum injection time, three microscans, and scan ranges of 585-640 *m/z* for histone H3 or 700-1400 *m/z* for histone H4 were used. For histone H3, the target precursor selected for MS2 fragmentation included all H3 peaks from GluC peptides and chose the top 6 most abundant *m/z*. ETD fragmentation at 18 ms reaction time, 1.0e6 reagent target with 200 ms injection time was used. MS2 acquisition was performed using the orbitrap with the 30k resolution setting, an AGC target of 5.0e5, a max injection time of 200 ms, a 'normal' scan range, and two microscans. For histone H4, an intensity threshold of 1e5 was set for the selection of ions for fragmentation. The target precursor selected for MS2 fragmentation included all major H4 peaks and chose the top 20 most abundant *m/z*. ETD fragmentation at a 14 ms reaction time, 5.0e5 reagent target with 200 ms injection time was used. MS2 acquisition was performed using the orbitrap with the 60k resolution setting, an AGC target of 5.0e5, a max injection time of 200 ms, a 'normal' scan range, and three microscans.

Mass spectrometry data analysis

For histone quantitation, 3-5 animals were analyzed in each of three different housing conditions, giving n=11-15 total for each organ/tissue. Two technical replicates were analyzed per sample and averaged to give the measured value for a minimum of three biological data points per group. Raw files were converted to .mzXML. Data processing

was performed by a custom analysis suite as previously described (41, 42). TDMS version 7.04 and Interp 2v15 were used for analysis. This data analysis approach has been used extensively in other studies in our lab to reveal quantitative changes in histone proteoforms (43, 44). For analyses of BAT versus liver histone modifications, we conducted multiple unpaired t-tests using the false discovery rate approach, and discoveries were determined using the two-stage linear step-up procedure of Benjamini, Krieger and Yekutieli. For all other analyses, Welch's 2-tailed t-tests or one-way ANOVA with Tukey posthoc testing were used when comparing two or three groups, respectively. *Q*-, *p*-, or p_{adj}- values less than 0.05 were considered statistically significant.

Fold- and absolute change: A fold change cutoff of 1.5 was also used; however, absolute change was also used to inform decisions on biological significance. Unlike many proteomic methods, we accurately measure absolute change. In our experience, it is not uncommon for large absolute changes to result in small-fold changes yet have profound biological significance. For example, a histone PTM that decorates 50% of the entire genome that increases to 70% results in a change to an astounding 20% of the genome but is less than 1.5-fold. Thus, consideration of both fold change and absolute change is insightful and represented as independent metrics.

Experimental Design and Statistical Rationale

Unless otherwise stated, experiments were designed with an N of 3-5 per group (BAT or liver from mice housed at TN, RT, and SC). The data obtained was interpreted collectively for a robust understanding of the system. Rigor was enhanced through multiple complimentary methods to understand epigenetic changes during BAT thermogenesis.

Mouse BAT Cold Stress

Various parametric statistics and corrections were used and are described above. Generally, one-way ANOVA with Tukey post-hoc testing or Welch's two-tailed t-tests were used with $p < 0.05$ considered statistically significant. P_{adj} or q values are calculated where appropriate, namely with consensus transcriptional regulatory network and RRBS analyses and comparisons between tissue histone modifications at each temperature.

Results

Analysis of RNA-Seq data reveals housing temperature-dependent effects on genes involved in epigenetic regulation. Acclimation and BAT remodeling in response to ambient temperatures occurs when mice are housed under constant temperatures for at least 7 days (45). Additionally, prior studies have established that standard laboratory housing of mice at 20-24°C is a chronic mild cold condition that stimulates NST (1, 45, 46). Expression of genes associated with histone acetylation, acetyl-CoA synthases *Acly* and *Acss2*, have been reported to increase in BAT in response to mild and severe chronic cold housing conditions (19). We reanalyzed and further interrogated the publicly-available RNA-Seq data deposited by Sanchez-Gurmaches *et al*. and noted significant cold housing temperature-induced reductions in the expression of genes encoding DNA methyltransferases, *Dnmt1*, *Dnmt3a*, and *Dnmt3b*, as well as altered expression of histone-modifying enzymes *Smyd3, Kdm2b, Setd7, Kdm3a, Kdm5b, Kdm5c*, and *Kdm8* (**Table 2**). In addition, we noted significantly altered expression of genes involved in one-carbon metabolism, suggesting that there may be housing temperature-dependent effects on the methyl donor pool that could also contribute to epigenetic modifications in BAT.

Regulatory network analysis resolves epigenetic writer footprints in cold challenge-regulated gene sets. High confidence transcriptional target (HCT) intersection analysis computes gene sets of interest against libraries of high confidence direct targets derived from public ChIP-Seq datasets to resolve regulatory footprints within those gene sets for transcription factors and other signaling nodes (28–31, 47). To identify

signaling nodes whose gain or loss of function contributed to the observed cold challenge expression profiles, we subjected genes significantly induced or repressed in each of the three contrasts to HCT intersection analysis (**Supplemental File S1**). As validation, we reasoned that our analysis should identify strong footprints within cold exposure-induced genes for nodes encoded by genes whose deletion in the mouse results in deficient thermoregulatory processes. To test this hypothesis, we retrieved a set of nodes (n=15) mapped to the null phenotype “impaired adaptive thermogenesis” (MP:0011049) or “abnormal circadian temperature homeostasis” (MP:0011020) from the Mouse Genome Database and designated these “thermoregulatory nodes.” We then evaluated the distribution of these thermoregulatory nodes among nodes that had strong regulatory footprints among cold challenge-induced genes in the three contrasts (**Figure 1A-C**) (26). Consistent with the reliability of our analysis, we observe strong enrichment of the thermoregulatory nodes among the top ranked cold-induced footprint nodes in all three experiments. These nodes include the nuclear receptors *Pparg*, *Ppara*, and *Esrra*, in addition to *Cebpb* and *Prdm16*, among others (48–52).

We next questioned whether the expression of epigenetic writers in BAT is altered in the response to different housing temperatures. We observe robust (FDR < 0.05) footprints within cold challenge-induced genes for numerous enzymes in the methyltransferase, demethylase, acetyltransferase and deacetylase classes, summarized in **Figure 1D**. These include nodes with characterized or inferred roles in thermal regulation, such as the acetyltransferases *Crebbp*/CBP, EP300/p300, and *Kat2a*/*Gcn5*; deacetylases such as members of the HDAC and sirtuin families; methyltransferase members of the KMT2 family as well as *Mettl3*; and the KDM family

demethylases (13, 53–61). We observe particularly strong footprints among cold challenge-induced genes for *Setd1a*, which has only recently been implicated in thermogenesis (62). In addition to these nodes, our analysis hints at roles for a number of nodes with no previously resolved role in the response to cold challenge, such as *Cdyl*, *Kat5*/TIP60, *Kat8*, *Ash2l*, *Ehmt2* and *Setdb1*.

Establishing a mouse model to interrogate the BAT epigenetic cold response. To investigate epigenetic changes in BAT due to chronic thermogenic activation in response to mild or severe cold housing temperatures, tissues were collected from 10-week-old mice housed under thermoneutral (TN, 28°C), room temperature (RT, 22°C), or, for the last two weeks of the study, severe cold (SC, 8°C) conditions. Our data support prior reports that lower housing temperatures are associated with significant reductions in adiposity, as we observe reduced end body weight, total fat mass, and weight of gonadal white adipose tissue in response to SC housing (63). There was no effect on nonfasting blood glucose levels, lean mass, or weights of BAT, liver, or spleen in our study (**Table S1**). Consistent with previous reports in hamsters and rats, kidney weight was inversely associated with housing temperature (64, 65).

DNA methylation and gene expression in BAT is altered in response to chronic thermogenic activation. DNA methylation at the promoters and first intron of genes is inversely correlated with gene expression, whereas intragenic DNA methylation may reduce spurious transcription and regulate the expression of alternate splice variants (66–69). To date, it is not known whether adaptation to cold induces large-scale epigenetic

changes to DNA that impact global expression of genes and their splice variants in BAT. Our reanalysis of publicly available RNA-Seq data yields numerous differentially expressed alternative splicing factors and alternative splice variants for BAT taken from SC- vs TN-housed mice, suggesting a potential role for differential methylation in the control of alternative splicing events (**Table 2, Figure 2A**, and **Supplemental Files S2 and S3**). To assess whether epigenetic modifications of DNA were occurring in BAT in response to chronic thermogenic activation, we first conducted reduced representation bisulfite sequencing (RRBS) using DNA extracted from BAT samples taken from mice housed under TN, RT, and SC temperature conditions. We noted 111 differentially hypomethylated and 18 differentially hypermethylated promoters; and 92 differentially hypomethylated and 16 differentially hypermethylated intragenic regions in BAT from RT-housed mice compared to TN-housed mice (**Figure 2B-D**). Housing at SC further increased the total number of differentially hypomethylated promoters and intragenic regions, while reducing the number of differentially hypermethylated promoters, when compared with TN. There are fewer total numbers of differentially methylated promoters and intragenic regions in BAT taken from mice housed under SC vs RT conditions. These data suggest that colder housing temperatures result in reduced DNA methylation in BAT, in general, and show that changes induced by SC vs RT are not as great as compared to SC vs TN or RT vs TN.

We next sought to identify genes with changes in promoter methylation that are inversely associated with gene expression, as this would suggest gene expression regulation as a result of altered DNA methylation. We integrated our RRBS data with the RNA-Seq data deposited by Sanchez-Gurmaches *et al*. from C57BL/6J wildtype mice

housed under similar conditions (**Table 3 and Supplemental File S3**) (46). In mice housed at RT vs TN, *Car8*, *Ndufb11*, *Vma21*, *Vldlr*, *Lyplal1*, and *Car13 showed* the greatest percent reduction in promotor methylation that was also associated with increased gene expression in BAT (percent methylation difference > |5|; 1.5-1.8-fold expression; p_{adj} <0.05). Conversely, increased promoter methylation for *Tpcn2* was associated with decreased expression (0.54-fold, percent methylation difference > |5|; 0.54-fold expression; p_{adj} <0.05). SC housing resulted in hypomethylation of additional promoters, including the promoters for *Dlg3*, *Uba1*, *Dnajc14*, and *Tspan31*, for which gene expression was also significantly increased (1.15-2.65-fold, percent methylation difference > |5|; 1.15-2.65-fold expression; p_{adj} <0.05). Although we observed significant differential methylation of promoters in BAT from SC- vs RT-housed mice, none were inversely associated with gene expression changes. Taken together, our results indicate that changes in DNA methylation in BAT are associated with chronic activation of the NST response and the more severe the chronic cold challenge, the greater the changes to DNA methylation.

Quantitative, proteoform-level data can be obtained from brown adipose tissue. A "proteoform" is a protein defined with chemical precision, including how combinations of PTMs co-occur in cis, on single molecules (70). Thus, quantitation of histone proteoforms accesses the true physiological state and simultaneously provides quantitation of associated discrete attributes such as histone PTMs. However, this has not been previously achieved for brown adipose tissue in any study to date. To analyze changes in histone modifications due to different housing temperatures, we first established

histone extraction methods for BAT. Well-established methods for histone extraction from liver, our benchmark tissue, were modified for BAT (19). Considering the high lipid content of BAT, we performed a matrix of experiments changing the percent detergent (NP-40, 0.3-1%), the number of times samples were incubated with detergent, the incubation time in detergent, the number of subsequent washes of nuclei, and the duration of centrifugation during nuclei isolation. Successful changes that are incorporated in this protocol include an additional sample incubation with detergent, an additional wash of nuclei, and a higher centrifugation duration compared to previously published protocols (19). A table summarizing histone yield with chosen experiments is shown in **Table S2**. Acid extraction was successful with no changes to the protocol. Once histones were isolated, offline HPLC was used to separate histone families and H3 variants and our published mass spectrometry methods could be used (19, 41). Our final workflow is shown in **Figure 3A**. We obtained adequate offline HPLC separation of histone family members yielding sufficient quantity for LC-MS/MS analysis (**Figure 3B, Table S3A**). This allows for very efficient histone extraction, yielding more histone per gram tissue than obtained with livers (**Figure 3C** and **Table S3B**). Once these histones were prepared and analyzed by mass spectrometry, we obtained high-quality chromatography, localization of PTMs, and quantitation of proteoforms (**Figure 3D-G**). Overall, this method obtains high-quality, quantitative data on histone proteoforms from limited tissue samples.

Quantitative analysis of histone post-translational modifications and proteoforms. There are two major innovations in this data: 1) quantitation of the stoichiometric

occupancy of histone PTMs and 2) quantitation of the single molecule co-occurrence of even distal modifications. Reporting and understanding these data require additional language, notation, and explanation. Most methods measure the increase or decrease of PTM signal relative to a starting condition. This leads to misunderstanding the stoichiometry and absolute abundance of PTMs. The more commonly discussed histone PTMs, such as K4me3 and K9ac, are among the least abundant and disproportionately not found alone but on single molecules in combination with other PTMs. The most abundant histone H3 PTMs are actually: K9me2, K27me2, K36me2, K14ac, and K23ac and are typically in the range of 25-40% stoichiometric occupancy (71). We also consider the quantitative stoichiometry of the unmodified state, “un”, as a potential signal. The unmodified state is often a low or even the least stoichiometrically abundant state.

Proteoforms are chemically defined single protein molecules, complete with all sources of variation (70). This includes how PTMs co-occur, in cis, on the same molecule and on which sequence variant (72). Thus, quantitative proteoform-level data presents a more complete description of the true physiological state of histone proteins (73). Contrary to common perceptions, histone H3 is rarely found in an unmodified state (~1%), single modification is uncommon (~10%), and multiple modifications (2+ PTMs) are abundant (~90%) (unpublished data). To distinguish PTMs and proteoforms we use curly brackets “{}” to indicate that the enclosed PTMs are present, and the abundance of all proteoforms that contain those modifications are summed. Angle brackets “<>” indicate that the enclosed PTMs are the only modifications on the histone protein save for N-terminal acetylation, with the abundance shown for that species. What may be considered contradictory PTM signals are often observed on the same molecule. For example,

H3<K9me2K14acK23acK27me3> is one of the most common states of histone H3 (71). Combinations of modifications also can obfuscate antibody-based detection and result in error (74). We generally take a reductionist approach to this complex higher dimension data. From this data we marginalize or reduce the dimensionality to individual PTMs or metrics such as bulk methylation and acetylation. However, we also derive complex insights that are otherwise not possible, such as single molecule binary combinations of PTMs.

Cold adaptation results in tissue-specific changes in total histone H3.2 and H4 acetylation and methylation. It has been previously reported that BAT *Acly* and *Acss2* expression is increased in response to mild and severe chronic cold stress, potentially resulting in an increased pool of acetyl-CoA available for histone modification (46). The observed housing temperature-dependent differences in the expression of genes involved in one-carbon metabolism in BAT further suggests that the pool of available methyl donor (S-adenosyl methionine, SAM) for histone modification may also be influenced by the degree of thermogenic activation (**Table 2**). Therefore, we sought to determine the effect of housing temperature on bulk histone acetylation and methylation in BAT. To understand the unique basal epigenetic state of BAT, we also analyzed histones from liver samples taken from the same animals for comparison. The percent of histone with one or more acetylations changes for both histone H3.2 and H4 in BAT (**Figure 4A**). Histone H3.2 with at least one acetylation is more abundant in BAT at SC compared to TN (45.2 and 35.6 percent H3.2 that has at least one non-N terminal acetyl group). Histone H3.2 acetylation in BAT is more abundant at RT compared to TN (43.1

and 35.6 percent acetylated). Histone H4 acetylation is also the most abundant in BAT at SC compared to TN (39.4 and 36.9 percent acetylated, $p = 0.03$) and SC compared to RT (39.4 and 36.8 percent that is acetylated, $p = 0.02$). However, there is no significant effect of housing temperature on bulk histone acetylation in liver. There are also no significant differences between tissues with histone H3.2 or H4 acetylation at each housing temperature. The percent of histones with at least one methylation did not change significantly with housing temperature or tissue type (**Figure 4B**). As noted above, these high stoichiometric occupancies are expected because H3 is physiologically hyper-modified and we are considering multiple sites of methylation in bulk. Our analysis approach allows for absolute quantitation and more directly reflects the stoichiometric use of the acetyl-CoA pool, the number of acetyl or methyl groups per histone molecule, and is shown in **Figure 4C** and **4D** respectively. Histone H3.2 acetylation follows a similar trend where SC BAT shows the highest acetylation levels, 0.63 acetylations per histone H3.2 molecule, except for liver at RT which is 0.65 acetylations per H3.2. There are large differences in acetylations per histone H3.2 molecule with a 0.12 difference between SC and TN housing and 0.10 difference between RT and TN housing. Histone H4 acetylation is highest in BAT from mice housed at SC, 0.46 acetylations per histone H4 molecule, and second highest in liver from mice housed at SC, 0.45 acetylations per H4 molecule. Taken together, our data show for the first time that bulk changes to histone acetylation and methylation with cold adaptation are tissue-specific.

Brown adipose tissue exhibits different histone PTMs and proteoforms than liver. We next sought to determine whether histone PTMs and proteoforms are different in BAT

versus liver. Here, we focus on significant differences at RT between tissues for discrete PTMs, binary PTM combinations, and proteoforms (**Figure 5 and Supplemental File S4**). However, the highest number of significant differences between tissues is at SC. In general, K9me3 and K36un and their combinations are more abundant in BAT compared to liver. Exceptions include {K27ac,K36un} at RT and {K27me3,K36un} at SC. At RT, BAT histone H3.2 shows significantly higher levels of PTMs K9me1, K9me3, K27me1, and K36un. Many differences are also observed between tissues for binary modifications and proteoforms in histone H3.2 (**Figure 5A** and **5D**). Because of our absolute quantitation, we can calculate the difference – not just fold change – in the abundance of particular modifications or proteoforms. This difference is indicative of the percent of the genome that is affected by the change in this proteoform (percentage point, pp). For example, H3.2<K9me2K27me1> is 1.7 percent abundant in the liver and 6.0 percent abundant in BAT, a 4.3 pp difference. Thus, the difference in abundance of H3.2<K9me2K27me1> affects a massive 4.3 percent of the genome when comparing liver and BAT at RT. For reference, the abundance of {K4me3} typically decorates less than one percent of the genome yet is crucial for active gene transcription (75). The largest absolute differences with significance are observed with the histone H3.2 proteoforms <K9me3K27me1>, <K9me2K27me1>, and <K9me2K27me3K36me1>. H3.2<K9me3K27me1> and <K9me2K27me1> are more abundant in BAT than in the liver. H3.2<K9me3K27me1> is 0.5 percent abundant in the liver and 3.3 percent abundant in BAT, affecting 2.7 percent of the genome. H3.2<K9me2K27me3K36me1> is more abundant in the liver than BAT (3.7 and 1.6 percent of total H3.2, respectively) and affects 2.1 percent of the genome. In

total, these proteoforms are responsible for a shift in 10.8 percent of the genome between BAT and liver.

Overall, histone H4 PTM changes are observed most frequently at SC (**Supplemental File S4**). This includes {K20me1} containing binary combinations and the otherwise unmodified proteoform <K20me1> which are more abundant in the liver compared to BAT. Histone H4 at RT shows no significant differences between tissues for discrete PTMs or binary PTM combinations, proteoform abundances (**Figure 5B** and **5E**) trend toward differences in BAT and liver. H4<K20me1> and <K20me2> are more abundant in liver than BAT. H4<K20me1> is 5.4 percent abundant in the liver and 4.7 percent abundant in BAT, changing 0.62 percent of the genome. H4<K20me2> is 39.4 percent abundant in the liver and 36 percent abundant in BAT, causing a shift in 3.4 percent of the genome while only 0.91-fold change. H4<K20me3> is more abundant in BAT than liver. H4<K20me3> is 19 percent abundant in the liver and 22 percent abundant in BAT, causing a shift in 2.5 percent of the genome. Overall, our results reveal tissue-specific discrete PTM abundances, PTM combinations, and proteoforms for histone H3.2, and to a lesser extent, H4 at RT housing.

BAT histone H3.2 changes with cold exposure are centered around K9me2 and K9un. Few temperature-dependent changes were observed in liver. Our motivating central hypothesis is that there is a BAT-specific epigenetic response to housing temperature. This is rationalized by the importance of histone PTMs in the regulation of transcription and the known unique physiological role of BAT in nonshivering thermogenesis. To determine epigenetic changes that occur during the cold response,

we analyzed discrete PTMs, PTM combinations, and proteoforms of histones in BAT from TN-, RT-, and SC-housed mice. Discrete PTM analysis of histone H3.2 shows significant increases in PTMs K9me2 and combined K9me2 and K9me3, {K9me2/3}; and decreased unmodified K9, {K9un}, in response to SC housing (**Figure 6A**). Histone H3.2 proteoforms shows trends in K9 di-methylation with K36 methylation (**Figure 6B)**. The presence of K9me2 or K9me3 and K36me1 on the same molecule is greatest at SC when combined with K23ac (**Figure 6C**). Supplemental data is available for further analysis (MassIVE: MSV000092105, **Supplemental File S5**). Our data indicate a role for altered histone H3.2 methylation and acetylation in the regulation of transcription in BAT in response to cold stress.

Histone H4 proteoforms in cold-adapted brown adipose tissue show highly specific changes including K16ac. We hypothesize that there are BAT-specific epigenetic changes with cold exposure that will affect histone H4 proteoforms. As with histone H3.2, we analyzed discrete PTMs, PTM combinations, and proteoforms for histone H4. We observe no significant histone H4 discrete PTM changes between BAT from mice housed at various temperatures. Interestingly, most H4 proteoforms that significantly change with housing temperature include K16ac, which may play a permissive role in the regulation of gene expression (**Figure 7A-B**) (76, 77). Further examination reveals specific proteoform changes, which includes <K12acK16acK20me1K31ac> and <K8acK16acK20me3>, both of which significantly increase at SC vs RT or SC vs TN (**Figure 7C** and **7D**)**.** Supplemental data is available for further analysis (MassIVE:

MSV000092105, **Supplemental File S6**). These results show that specific histone H4 proteoforms increase in BAT in response to chronic cold.

Discussion

Our data reveal novel housing temperature-dependent, gene expression and tissue-specific epigenetic changes in brown adipose tissue. Interrogating a publicly available BAT RNA-Seq dataset, we observe significant temperature-dependent changes in the expression of genes that regulate one-carbon metabolism, DNA methylation, histone modification, and alternative splicing. Further interrogation of the RNA-Seq dataset uncovers a number of alternative splice variants that are differentially expressed at TN vs SC housing. Our RRBS data from BAT reveals less DNA methylation at promoter and first intronic regions and intragenic regions, and this is associated with reduced *Dnmt1*, *Dnmt3a*, and *Dnmt3b* expression, with colder housing temperatures. We developed a method for the efficient extraction of histones from BAT that allows for top-down quantitation of proteoforms in BAT in an unbiased manner. This enables exploration of housing temperature-associated epigenetic changes in BAT. A comparison between BAT and liver reveals tissue-specific, housing temperature-dependent changes in histone proteoforms. Consistent with a functional effect of increased *Acly* and *Acss2* expression in BAT, we observe increases in H3.2 and H4 total acetylation in BAT, but not in liver, in response to severe chronic cold. Housing temperature had no effect on total methylation levels of histones H3.2 and H4 in either BAT or liver. Further examination reveals tissue-specific housing temperature-dependent changes in histone H3.2 and H4 PTMs and proteoforms in BAT. Our data show for the first time that chronic severe cold housing results in large-scale epigenetic changes to both DNA and histones in murine BAT, and that housing temperature affects histone modifications in liver, albeit to a lesser extent.

Housing Temperature Alters DNA Methylation in BAT

This is the first report of global thermogenesis-associated DNA methylation changes in BAT. Using RRBS, we discovered decreasing DNA methylation in BAT as housing temperature decreases. This may be due to reductions in DNA methyltransferase activity, as RNA-seq reveals lower expression of *Dnmt1*, *Dnmt3a*, and *Dnmt3b* at both SC and RT compared to TN (11, 66, 67, 78, 79). Intriguingly, DNMT1 represses myogenic remodeling of BAT, and inhibits the expression of adiponectin (*Adipoq*) by adipocytes (11, 80). In spite of this, RNA-seq results indicate that BAT expression of *Adipoq*, which has been shown to inhibit BAT thermogenesis, is significantly reduced by SC compared with RT or TN housing conditions (46, 81). We also found no housing temperature-mediated association between *Adipoq* expression and DNA methylation at the adiponectin promoter, suggesting that DNMT1 activity does not play a major role in the regulation of *Adipoq* expression during chronic severe cold stress. DNMT3a regulates adipocyte differentiation, and DNMT3a deficiency reduces both lipogenesis and lipolysis *in vitro* (78). DNMT3b deficiency in Myf5^{+} brown adipocyte precursor cells impairs the thermogenic program and upregulation of myogenic gene expression in female mice (79). However, these studies of the role of DNA methyltransferases in adipocytes do not address effects of reduced DNMT activity caused by environmental factors, such as housing temperature, in already differentiated adipocytes. Further studies are warranted with regard to the roles of DNA methyltransferases in differentiated BAT in response to chronic cold.

We also report novel findings from integration of our RRBS data with publicly-available RNA-seq data. Interestingly, the genes with the greatest reductions in promoter

methylation for which expression is also increased in response to chronic cold stress included genes recently reported to play an important role in fatty acid uptake by thermogenically active BAT, *Vldlr*, and in mitochondrial electron transport, *Ndufb11* (82, 83). Of note, BAT *Vldlr* expression and uptake of VLDL increase in response to cold stress, and VLDLR deficiency impairs thermogenesis in mice (82). As VLDLR also facilitates the uptake of fatty acids from chylomicrons via lipoprotein lipase-mediated triglyceride hydrolysis, increased *Vldlr* expression represents a means through which cold stress may promote the uptake of fatty acids from circulating chylomicrons postprandially, as well (84). Our results suggest that alterations in DNA methylation at promoters is one mechanism through which gene expression for optimal nutrient utilization during thermogenesis is regulated in BAT in response to prolonged cold stress.

Methylation of intragenic regions of DNA differentially affects the expression of alternative splice variants and modification of histones (69, 85). Our analysis of publicly-available RNA-seq data yields a number of alternative splice variants that are differentially expressed in BAT at SC vs TN. Additionally, analysis of RNA-seq data reveals associated increased expression of HuR/*Elavl1* and *Igf2bp2*, and decreased expression *Nova2*, *Pspc1*, and many serine-arginine rich splicing factors in BAT from mice housed at SC vs TN. This suggests that expression of RNA-binding proteins known to mediate alternative splicing in adipose tissues are also altered during chronic cold stress (86–88). Our results indicate the need for further studies to better characterize the mechanism(s) driving housing temperature-associated alternative splicing events in BAT, as well as the biological function of alternative splice variants that are expressed in BAT in response to chronic cold stress.

Here we also describe a number of housing temperature-dependent histone modifications, particularly H3{K9me2} and H3{K9me3}, which have been previously associated with methylated DNA (89–91). Overall, our results show that chronic cold stress affects DNA methylation in BAT, and that this may play a role in larger changes to the transcript profile in BAT through effects on transcription and splicing. The major limitations of RRBS are that the method can only assess methylation at 10-15% of all CpG sites in the genome and that it cannot distinguish between 5-methylcytosine and its demethylation intermediate, 5-hydroxymethylcytosine (92–94). Future studies will utilize whole genome bisulfite sequencing for a more comprehensive approach to thermogenically-responsive changes in DNA methylation in BAT.

Our Data Reveal the First Top-down Quantitative Look at Histone Modifications in Murine BAT

Top- or middle- down mass spectrometry-based methods are ideal for the identification and quantitation of histone PTMs (73, 95–100). Due to their proximity and role in the regulation of the genome, changes in histones can have dramatic or small but significant effects on the physiology of the genome. PTMs on histones such as acetylation, methylation, and phosphorylation are well-known to affect the binding of other factors and have a wide range of downstream activities (43, 101, 102). Histone modifications are known to function in concert on single molecules and are described in more detail in a recent review of histone PTM combinations (73). The method we describe here allows for quantitative statistical analysis of changes in histone modifications and proteoforms in BAT for the first time, thus providing information on the true physiological

state of histones including all co-occurring modifications. Furthermore, this method provides absolute quantitation of proteoforms and PTMs, which is useful for understanding the biological significance of the changes. While our method measures proteoforms, the discrete abundance of PTMs is obtained through marginalization. This differs from other techniques such as antibody-based techniques where only one modification can be probed at a time or from bottom-up mass spectrometry techniques where distal co-occurring modifications usually cannot be measured. Furthermore, most antibody-based studies poorly differentiate between di- and tri-methylation (59, 60).

There is a growing body of literature establishing mechanisms of chromatin regulation that operate at the proteoform level (43, 70, 71, 75, 96, 101, 103, 104). However, most prior work in chromatin and epigenetics ascribes function to discrete single PTMs. Marginalizing modifications from top-down analysis can both reveal minimal functional units within each proteoform and enable comparison to prior methodologically limited literature. This brings in important concepts such as “discrete” PTMs, the presence or absence of a single PTM, “binary combinations” of PTMs, the presence or absence of two PTMs, and the proteoform which considers all PTMs on the histone molecule. We also considered the unmodified state, denoted as “un”, as its own modification state.

Method development considerations for successful extraction of histones from BAT include lipid content and complexity of tissue. Isolation of nuclei from tissue presents many challenges due to the complexity of the sample compared to tissue culture. However, we have recently published methods to overcome issues in most types of tissue (19, 40). BAT presents unique challenges due to its high lipid content that proves current methods unsuccessful (18). Here we modify nuclear isolation methods to remove excess

lipids, and complete a matrix of experiments to optimize BAT nuclei isolation. Upon obtaining a pellet of BAT nuclei, we use established methods for the acid extraction of histones and analysis of histone proteoforms by mass spectrometry (41). Our method can be used for future studies of BAT histone proteoforms and their effects on nonshivering thermogenesis.

BAT and Liver are Epigenetically Distinct

Our analysis of bulk acetylation and methylation of histones H3.2 and H4 in BAT and liver from mice housed at different temperatures reveals tissue-specific responses to cold. Histones are generally the most acetylated at SC compared to other housing temperatures in BAT, with statistically significant changes in the percent of histone H4 that has more than one acetyl group. However, in liver there is no significant effect of housing temperature on acetylated histone levels. We observe no statistically significant histone H3.2 or H4 bulk methylation changes in either tissue. Differences in methyl groups per histone molecule are most affected by the histone identity (number of methylation sites) than housing temperature or tissue.

Although our focus for comparison of these tissues was RT housing temperature, we observe the greatest number of significant changes in single PTMs, 2-PTM combinations, and proteoforms at SC. The significantly differing combinations containing H3.2{K9me3} are always more abundant in BAT compared to liver, regardless of housing temperature. This indicates transcriptional repression of genes through HP1 in BAT (105). The abundance of H3.2{K36un} and combinations including K36un are typically more abundant in BAT compared to liver, consistent with decreased deposition of K36

methylation during transcription (106). Thus, there is more K9 methylation to recruit HP1, which would result in less transcription and less co-transcriptional methylation of K36. Fewer differences between tissues are observed with histone H4 but center on {K20me1} at SC. H4{K20me1} binary combinations and H4<K20me1> are more abundant in the liver. Generally, we observe PTM changes between tissues that indicate less active transcription in BAT.

At RT, histone H3.2 proteoforms that are significantly more abundant in BAT than liver are H3.2<K9me2K27me1>, H3.2<K9me3K27me1>, H3.2<K9me3>, and H3.2<K9me2> and indicate an increase in heterochromatin in BAT (102, 107). Histone H4 proteoforms H4<K20me3>, H4<K16acK20me2>, and H4<K16acK20me3> trend toward greater abundance in BAT compared to liver. These proteoforms indicate transcriptional repression or a poised state (108). H4<K20me2> and H4<K20me1> are significantly more abundant in liver than BAT and are associated with transcriptional activation (109). H4<K20me2> is 39 percent of all H4 in liver and 36 percent abundant in BAT, affecting 3.4 percent of the genome. H4<K20me1> is 5.4 percent of all histone H4 in liver and 4.7 percent abundant in BAT. Significant discrete changes between tissues are observed in histone H3.2 but not histone H4 at RT. The changes in proteoform abundances reflect poised positions that act as a scaffold for other factors that determine downstream effects (43). These proteoforms are often quite abundant in tissues and cultured cells and their shift indicates an upstream broad difference between tissue epigenetic regulation (41, 43). Significantly changing proteoforms of histone H3.2 and H4 indicate higher levels of heterochromatin in BAT compared to liver at RT (102, 107–109). Histone modifying pair p300/CBP is crucial to adipogenesis and their activity is necessary

for the expression of all the pan-adipocyte genes (53). Our histone findings suggest that p300/CBP activity is lower in BAT compared to liver, consistent with fewer genes being expressed in BAT compared to liver.

Housing Temperature Affects Histone Modifications in BAT

Our data show that BAT responds epigenetically to cold stimuli and further reveal changes in its epigenome that may drive its function during cold adaptation. Bulk histone acetylation increases in BAT from SC- vs TN-housed mice, while there is no change in bulk methylation associated with differences in housing temperature. This is consistent with changes in gene expression upon cold challenge. Expression of *Acss2* and *Chrebp (Mlxipl)* and its known target *Acly* increase in BAT when mice are housed under chronic mild and severe cold conditions (46, 110). ACLY and ACSS2 provide acetyl-CoA for histone acetylation through citrate and acetate, respectively, and their upregulation provides potential mechanisms for our findings. Additionally, carnitine acetyltransferase (CrAT) and carnitine octanoyltransferase (CrOT) have both been shown to play important roles in the ACLY- and ACSS2-independent conversion of short- and medium-chain acetylcarnitines to acetyl-CoA (111, 112). Analysis of RNA-seq data reveals that both *Crat* and *Crot* expression increase in BAT during chronic cold housing, suggesting additional mechanisms through which BAT activation generates acetyl-CoA that can be used for post-translational modification of histones. Indeed, histone H4 and H3.2 acetylation sites are the most occupied at SC in BAT, indicating a shift in BAT acetyl-CoA pools. Our data are consistent with increased intracellular acetyl-CoA levels under conditions of chronic cold contributing to increasing histone acetylation.

Mouse BAT Cold Stress

Histone post-translational modifications (PTMs) suggest a mechanism through which temperature-dependent selective transcription in BAT may occur. Either the presence or absence of PTMs can be biological signals. Under SC conditions, histone H3.2 {K9me2} and {K9me2/3} increase and {K9un} decrease, suggesting a repressive transcriptional signal (102, 107). However, further investigation into the K9me2 mark reveal changes with K36 methylation (K36me1 and K36me2) (61). This combination of PTMs is permissive of absolute transcriptional repression of certain genes while others are transcribed. The decrease in {K9un} supports this model. While the lack of commercially available {K9un} antibodies means there are few studies implicating function, a reasonable interpretation of loss of {K9un} is a shift away from a more transcriptionally permissive but still poised state. {K9un} is directly prone to either acetylation (activation) or methylation (repression) without erasure of the antagonistic mark (107, 113). As housing temperatures decrease, histone H4 proteoforms with K16ac increase. Importantly, {K16ac} acts as a scaffold and recruits factors for transcriptional activation (73). Mechanistically, H4{K20me2} promotes {K16ac} and further rapid acetylation in *cis* at K12, K8, and K5 (43). Taken together, histone H3 PTMs indicate persistent transcriptional repression of certain genes (through methylation) and histone H4 PTMs suggest an overall transient or poised state of transcription (through acetylation) in BAT when mice are housed at colder temperatures. Our findings suggest that housing temperature in conjunction with nutrient intake modifies acetyl-CoA availability and is reflected in histone PTMs concomitant with methylation-dependent gene repression in BAT.

Mouse BAT Cold Stress

Our gene expression and transcriptional footprint analyses suggests a potential mechanism by which methylation-dependent gene repression in BAT may occur. Overall, RNA-seq analysis reveals that *Fcor* expression increases under SC compared to TN housing conditions. However, *Fcor* expression is induced to a greater extent under mild compared to severe cold conditions (RT vs SC). FCOR regulates FOXO1 activity through repressive acetylation, during which a complex of FCOR and acetylated FOXO1 translocate to the cytosol (114). Additionally, we observe an increased SIRT6 transcriptional footprint under colder housing temperatures. SIRT6 deacetylates FOXO1, and SIRT1 deacetylates SIRT6, thus increasing SIRT6 activity (115, 116). When not acetylated, FOXO1 forms a complex with SIRT1 and can mediate the expression of SIRT1 (114, 117). Both SIRT1 and SIRT6 are known H3{K9ac} and {K56ac} deacetylases (118). SIRT1 is also known to deacetylate SUV39H1{K266ac} and H4{K16ac} (102, 113, 119). Deacetylation of H3K9 allows for other modifications at this site including H3{K9me2} or H3{K9me3} (113). Deacetylation of SUV39H1 lysine 266 by SIRT1 results in activation of this H3K9 dimethyltransferase and more H3{K9me3} (102). Additionally, H3K9 dimethylation can also result from demethylation of H3{K9me3}. KDM4C demethylates H3{K9me3} and its footprint increases upon cold challenge (120). Regardless if K9 methylation arises from writing or erasing, H3K9 trimethylation allows for binding of HP1, which results in repression of transcription and activation of a feedback loop with SUV39H1 (105, 121). The dramatically higher levels of {K9me2} at SC may result from increased KDM4C-mediated demethylase activity or SIRT1-regulated SUV39H1-mediated methyltransferase activity in BAT. Together, FCOR, FOXO1, SIRT6, SIRT1, KDM4C, and SUV39H1 may be involved in a complex system that activates upon

cold challenge in BAT. Collectively, our data imply a transcriptionally repressive feedback loop with {K9me2/3} and HP1 with cold challenge. Future work is required to fully elucidate specific mechanisms of epigenetic regulation in BAT.

In summary, we observe a BAT-specific epigenetic response to cold stress. Our data indicate a change in epigenetic regulation upon cold challenge and this is reflected in epigenetic writer transcriptional footprints, transcription of certain genes, DNA methylation, and combinations of histone modifications. This system includes multiple levels of regulation and complex feedback loops that are not well understood. While some of these observed shifts correlate well, others are more enigmatic. For example, the footprints of many histone modifying proteins including both writers and erasers increase upon cold challenge. Overall, our aim is to contextualize these findings while presenting our data as a resource for further studies. In summary, we provide the first unbiased look at the relative abundance of BAT histone proteoforms and their dynamic response to cold stress. Rationalization of some of these findings is possible through the current body of knowledge; however, fully understanding these responses will require future investigation.

Acknowledgments

B.C.T. and N.L.Y. were supported by NIH Grants R01 GM139295, P01 AG066606, RF1 AG074540, R01 CA193235, R01 CA276663, and R56 HG012206. M.D., H.K.Y., and G.E.Z. and N.R.M. were supported by United States Department of Agriculture (USDA/ARS) Cooperative Agreement No. 58-3092-0-001. H.K.Y. was additionally supported by a Duncan NRI Zoghbi Scholar Award to H.K.Y. S.A.O. and N.J.M. were supported by NIDDK Information Network Grant U24DK097771. A.M.N.-A. was supported by American Heart Association Career Development Award 18CDA34110137, USDA-ARS Cooperative Agreement 3092-51000-064-005-S, and a Texas Children's Hospital Pediatrics Pilot Award. The contents of this work are solely the responsibility of the authors and do not necessarily represent the official views of the USDA.

Author Contributions

B.C.T., N.L.Y., H.K.Y., N.J.M., and A.M.N.-A. conceptualization; B.C.T., L.H.S., M.D., H.K.Y., S.A.O., G.E.Z., N.R.M., N.J.M., N.L.Y., and A.M.N.-A. methodology and investigation; B.C.T., M.D., H.K.Y., S.A.O., N.J.M., and A.M.N.-A. formal analyses; B.C.T., M.D., N.J.M., N.L.Y. and A.M.N.-A. writing-original manuscript; N.L.Y. and A.M.N.-A. supervision and funding acquisition.

Data Availability

RRBS data are deposited in GEO (accession number GSE234588). Histone H3.2 and H4 mass spectrometry raw data are uploaded to the MassIVE repository (ftp://massive.ucsd.edu/MSV000092105/). All other data described in this manuscript are contained within the manuscript or as associated supplementary material.

Supplemental data

This article contains supplemental data. Additional supplemental files are available upon request.

References

1. Cannon, B., and Nedergaard, J. (2004) Brown Adipose Tissue: Function and Physiological Significance. *Physiol. Rev.* 84, 277–359

2. Lidell, M. E. (2019) Brown Adipose Tissue in Human Infants. *Handb. Exp. Pharmacol.* 251, 107–123

3. Cypess, A. M., Lehman, S., Williams, G., Tal, I., Rodman, D., Goldfine, A. B., Kuo, F. C., Palmer, E. L., Tseng, Y.-H., Doria, A., Kolodny, G. M., and Kahn, C. R. (2009) Identification and importance of brown adipose tissue in adult humans. *N. Engl. J. Med.* 360, 1509–1517

4. Orava, J., Nuutila, P., Lidell, M. E., Oikonen, V., Noponen, T., Viljanen, T., Scheinin, M., Taittonen, M., Niemi, T., Enerbäck, S., and Virtanen, K. A. (2011) Different metabolic responses of human brown adipose tissue to activation by cold and insulin. *Cell Metab.* 14, 272–279

5. Cypess, A. M., Doyle, A. N., Sass, C. A., Huang, T. L., Mowschenson, P. M., Rosen, H. N., Tseng, Y.-H., Palmer, E. L., and Kolodny, G. M. (2013) Quantification of human and rodent brown adipose tissue function using 99mTc-methoxyisobutylisonitrile SPECT/CT and 18F-FDG PET/CT. *J. Nucl. Med. Off. Publ. Soc. Nucl. Med.* 54, 1896–1901

6. van Marken Lichtenbelt, W. D., Vanhommerig, J. W., Smulders, N. M., Drossaerts, J. M. A. F. L., Kemerink, G. J., Bouvy, N. D., Schrauwen, P., and Teule, G. J. J. (2009) Cold-activated brown adipose tissue in healthy men. *N. Engl. J. Med.* 360, 1500–1508

7. Saito, M., Okamatsu-Ogura, Y., Matsushita, M., Watanabe, K., Yoneshiro, T., Nio-Kobayashi, J., Iwanaga, T., Miyagawa, M., Kameya, T., Nakada, K., Kawai, Y., and Tsujisaki, M. (2009) High incidence of metabolically active brown adipose tissue in healthy adult humans: effects of cold exposure and adiposity. *Diabetes* 58, 1526–1531

8. Chondronikola, M., Volpi, E., Børsheim, E., Porter, C., Annamalai, P., Enerbäck, S., Lidell, M. E., Saraf, M. K., Labbe, S. M., Hurren, N. M., Yfanti, C., Chao, T., Andersen, C. R., Cesani, F., Hawkins, H., and Sidossis, L. S. (2014) Brown adipose tissue improves whole-body glucose homeostasis and insulin sensitivity in humans. *Diabetes* 63, 4089–4099

9. Blondin, D. P., Labbé, S. M., Noll, C., Kunach, M., Phoenix, S., Guérin, B., Turcotte, É. E., Haman, F., Richard, D., and Carpentier, A. C. (2015) Selective Impairment of Glucose but Not Fatty Acid or Oxidative Metabolism in Brown Adipose Tissue of Subjects With Type 2 Diabetes. *Diabetes* 64, 2388–2397

10. Cypess, A. M., and Kahn, C. R. (2010) Brown fat as a therapy for obesity and diabetes. *Curr. Opin. Endocrinol. Diabetes Obes.* 17, 143–149

11. Li, F., Jing, J., Movahed, M., Cui, X., Cao, Q., Wu, R., Chen, Z., Yu, L., Pan, Y., Shi, H., Shi, H., and Xue, B. (2021) Epigenetic interaction between UTX and DNMT1 regulates diet-induced myogenic remodeling in brown fat. *Nat. Commun.* 12, 6838

12. Li, F., Cui, X., Jing, J., Wang, S., Shi, H., Xue, B., and Shi, H. (2021) Brown Fat Dnmt3b Deficiency Ameliorates Obesity in Female Mice. *Life Basel Switz.* 11, 1325

13. Emmett, M. J., Lim, H.-W., Jager, J., Richter, H. J., Adlanmerini, M., Peed, L. C., Briggs, E. R., Steger, D. J., Ma, T., Sims, C. A., Baur, J. A., Pei, L., Won, K.-J., Seale, P., Gerhart-Hines, Z., and Lazar, M. A. (2017) Histone deacetylase 3 prepares brown adipose tissue for acute thermogenic challenge. *Nature* 546, 544–548

14. Gerhart-Hines, Z., Dominy, J. E., Blättler, S. M., Jedrychowski, M. P., Banks, A. S., Lim, J.-H., Chim, H., Gygi, S. P., and Puigserver, P. (2011) The cAMP/PKA Pathway Rapidly Activates SIRT1 to Promote Fatty Acid Oxidation Independently of Changes in NAD+. *Mol. Cell* 44, 851–863

15. Boutant, M., Joffraud, M., Kulkarni, S. S., García-Casarrubios, E., García-Roves, P. M., Ratajczak, J., Fernández-Marcos, P. J., Valverde, A. M., Serrano, M., and Cantó, C. (2015) SIRT1 enhances glucose tolerance by potentiating brown adipose tissue function. *Mol. Metab.* 4, 118–131

16. Qiang, L., Wang, L., Kon, N., Zhao, W., Lee, S., Zhang, Y., Rosenbaum, M., Zhao, Y., Gu, W., Farmer, S. R., and Accili, D. (2012) Brown Remodeling of White Adipose Tissue by SirT1-Dependent Deacetylation of Pparγ. *Cell* 150, 620–632

17. Lim, S., Honek, J., Xue, Y., Seki, T., Cao, Z., Andersson, P., Yang, X., Hosaka, K., and Cao, Y. (2012) Cold-induced activation of brown adipose tissue and adipose angiogenesis in mice. *Nat. Protoc.* 7, 606–615

18. Strzyz, P. (2016) Lipid droplet growth in brown fat. *Nat. Rev. Mol. Cell Biol.* 17, 3–3

19. Holt, M. V., Wang, T., and Young, N. L. (2021) Expeditious Extraction of Histones from Limited Cells or Tissue Samples and Quantitative Top-Down Proteomic Analysis. *Curr. Protoc.* 1,

20. Leinonen, R., Sugawara, H., Shumway, M., and on behalf of the International Nucleotide Sequence Database Collaboration (2011) The Sequence Read Archive. *Nucleic Acids Res.* 39, D19–D21

21. Andrews, S. (2010) FastQC: a quality control tool for high throughput sequence data.

22. Dobin, A., Davis, C. A., Schlesinger, F., Drenkow, J., Zaleski, C., Jha, S., Batut, P., Chaisson, M., and Gingeras, T. R. (2013) STAR: ultrafast universal RNA-seq aligner. *Bioinformatics* 29, 15–21

23. Ewels, P., Magnusson, M., Lundin, S., and Käller, M. (2016) MultiQC: summarize analysis results for multiple tools and samples in a single report. *Bioinformatics* 32, 3047–3048

24. Love, M. I., Huber, W., and Anders, S. (2014) Moderated estimation of fold change and dispersion for RNA-seq data with DESeq2. *Genome Biol.* 15, 550

25. Shen, S., Park, J. W., Lu, Z., Lin, L., Henry, M. D., Wu, Y. N., Zhou, Q., and Xing, Y. (2014) rMATS: robust and flexible detection of differential alternative splicing from replicate RNA-Seq data. *Proc. Natl. Acad. Sci. U. S. A.* 111, E5593-5601

26. Blake, J. A., Baldarelli, R., Kadin, J. A., Richardson, J. E., Smith, C. L., Bult, C. J., and Mouse Genome Database Group (2021) Mouse Genome Database (MGD): Knowledgebase for mouse-human comparative biology. *Nucleic Acids Res.* 49, D981–D987

27. Smith, C. L., and Eppig, J. T. (2009) The mammalian phenotype ontology: enabling robust annotation and comparative analysis. *Wiley Interdiscip. Rev. Syst. Biol. Med.* 1, 390–399

28. Ochsner, S. A., Pillich, R. T., and McKenna, N. J. (2020) Consensus transcriptional regulatory networks of coronavirus-infected human cells. *Sci. Data* 7, 314

29. Zapata, R. C., Chaudry, B. S., Valencia, M. L., Zhang, D., Ochsner, S. A., McKenna, N. J., and Osborn, O. (2021) Conserved immunomodulatory transcriptional networks underlie antipsychotic-induced weight gain. *Transl. Psychiatry* 11, 405

30. Bissig-Choisat, B., Alves-Bezerra, M., Zorman, B., Ochsner, S. A., Barzi, M., Legras, X., Yang, D., Borowiak, M., Dean, A. M., York, R. B., Galvan, N. T. N., Goss, J., Lagor, W. R., Moore, D. D., Cohen, D. E., McKenna, N. J., Sumazin, P., and Bissig, K.-D. (2021) A human liver chimeric mouse model for non-alcoholic fatty liver disease. *JHEP Rep.* 3, 100281

31. Chen, K. Y., De Angulo, A., Guo, X., More, A., Ochsner, S. A., Lopez, E., Saul, D., Pang, W., Sun, Y., McKenna, N. J., and Tong, Q. (2022) Adipocyte-Specific Ablation of PU.1 Promotes Energy Expenditure and Ameliorates Metabolic Syndrome in Aging Mice. *Front. Aging* 2, 803482

32. Ochsner, S. A., Abraham, D., Martin, K., Ding, W., McOwiti, A., Kankanamge, W., Wang, Z., Andreano, K., Hamilton, R. A., Chen, Y., Hamilton, A., Gantner, M. L., Dehart, M., Qu, S., Hilsenbeck, S. G., Becnel, L. B., Bridges, D., Ma'ayan, A., Huss, J. M., Stossi, F., Foulds, C. E., Kralli, A., McDonnell, D. P., and McKenna, N.

J. (2019) The Signaling Pathways Project, an integrated ‘omics knowledgebase for mammalian cellular signaling pathways. *Sci. Data* 6, 252

33. Oki, S., Ohta, T., Shioi, G., Hatanaka, H., Ogasawara, O., Okuda, Y., Kawaji, H., Nakaki, R., Sese, J., and Meno, C. (2018) ChIP-Atlas: a data-mining suite powered by full integration of public ChIP-seq data. *EMBO Rep.* 19, e46255

34. Benjamini, Y., and Hochberg, Y. (1995) Controlling the False Discovery Rate: A Practical and Powerful Approach to Multiple Testing. *J. R. Stat. Soc. Ser. B Methodol.* 57, 289–300

35. Krueger, F., and Andrews, S. R. (2011) Bismark: a flexible aligner and methylation caller for Bisulfite-Seq applications. *Bioinformatics* 27, 1571–1572

36. Langmead, B., and Salzberg, S. L. (2012) Fast gapped-read alignment with Bowtie 2. *Nat. Methods* 9, 357–359

37. Akalin, A., Kormaksson, M., Li, S., Garrett-Bakelman, F. E., Figueroa, M. E., Melnick, A., and Mason, C. E. (2012) methylKit: a comprehensive R package for the analysis of genome-wide DNA methylation profiles. *Genome Biol.* 13, R87

38. Liao, Y., Wang, J., Jaehnig, E. J., Shi, Z., and Zhang, B. (2019) WebGestalt 2019: gene set analysis toolkit with revamped UIs and APIs. *Nucleic Acids Res.* 47, W199–W205

39. Walter, W., Sánchez-Cabo, F., and Ricote, M. (2015) GOplot: an R package for visually combining expression data with functional analysis. *Bioinformatics* 31, 2912–2914

40. Taylor, B. C., and Young, N. L. (2023) Histone H4 proteoforms and post-translational modifications in the Mus musculus brain with quantitative comparison of ages and brain regions. *Anal. Bioanal. Chem.* 415, 1627–1639

41. Holt, M. V., Wang, T., and Young, N. L. (2019) High-Throughput Quantitative Top-Down Proteomics: Histone H4. *J. Am. Soc. Mass Spectrom.* 30, 2548–2560

42. DiMaggio, P. A., Young, N. L., Baliban, R. C., Garcia, B. A., and Floudas, C. A. (2009) A Mixed Integer Linear Optimization Framework for the Identification and Quantification of Targeted Post-translational Modifications of Highly Modified Proteins Using Multiplexed Electron Transfer Dissociation Tandem Mass Spectrometry. *Mol. Cell. Proteomics* 8, 2527–2543

43. Wang, T., Holt, M. V., and Young, N. L. (2018) Early butyrate induced acetylation of histone H4 is proteoform specific and linked to methylation state. *Epigenetics* 13, 519–535

44. Jiang, T., Hoover, M. E., Holt, M. V., Freitas, M. A., Marshall, A. G., and Young, N. L. (2018) Middle-Down Characterization of the Cell Cycle Dependence of Histone H4 Posttranslational Modifications and Proteoforms. *PROTEOMICS* 18, 1700442

45. Virtue, S., and Vidal-Puig, A. (2013) Assessment of brown adipose tissue function. *Front. Physiol.* 4, 128

46. Sanchez-Gurmaches, J., Tang, Y., Jespersen, N. Z., Wallace, M., Martinez Calejman, C., Gujja, S., Li, H., Edwards, Y. J. K., Wolfrum, C., Metallo, C. M., Nielsen, S., Scheele, C., and Guertin, D. A. (2018) Brown Fat AKT2 Is a Cold-Induced Kinase that Stimulates ChREBP-Mediated De Novo Lipogenesis to Optimize Fuel Storage and Thermogenesis. *Cell Metab.* 27, 195-209.e6

47. Ochsner, S. A., Pedroza, M., Pillich, R. T., Krishnan, V., Konicek, B. W., Dow, E. R., Park, S. Y., Agarwal, S. K., and McKenna, N. J. (2023) IL17A blockade with ixekizumab suppresses MuvB signaling in clinical psoriasis. *J. Invest. Dermatol.*, S0022-202X(23)01941–3

48. Ahmadian, M., Abbott, M. J., Tang, T., Hudak, C. S. S., Kim, Y., Bruss, M., Hellerstein, M. K., Lee, H.-Y., Samuel, V. T., Shulman, G. I., Wang, Y., Duncan, R. E., Kang, C., and Sul, H. S. (2011) Desnutrin/ATGL is regulated by AMPK and is required for a brown adipose phenotype. *Cell Metab.* 13, 739–748

49. Carmona, M. C., Hondares, E., Rodríguez de la Concepción, M. L., Rodríguez-Sureda, V., Peinado-Onsurbe, J., Poli, V., Iglesias, R., Villarroya, F., and Giralt, M. (2005) Defective thermoregulation, impaired lipid metabolism, but preserved adrenergic induction of gene expression in brown fat of mice lacking C/EBPbeta. *Biochem. J.* 389, 47–56

50. Villena, J. A., Hock, M. B., Chang, W. Y., Barcas, J. E., Giguère, V., and Kralli, A. (2007) Orphan nuclear receptor estrogen-related receptor alpha is essential for adaptive thermogenesis. *Proc. Natl. Acad. Sci. U. S. A.* 104, 1418–1423

51. Harms, M. J., Ishibashi, J., Wang, W., Lim, H.-W., Goyama, S., Sato, T., Kurokawa, M., Won, K.-J., and Seale, P. (2014) Prdm16 is required for the maintenance of brown adipocyte identity and function in adult mice. *Cell Metab.* 19, 593–604

52. Shen, Y., Su, Y., Silva, F. J., Weller, A. H., Sostre-Colón, J., Titchenell, P. M., Steger, D. J., Seale, P., and Soccio, R. E. (2020) Shared PPARα/γ Target Genes Regulate Brown Adipocyte Thermogenic Function. *Cell Rep.* 30, 3079-3091.e5

53. Namwanje, M., Liu, L., Chan, M., Aaron, N., Kraakman, M. J., and Qiang, L. (2019) The depot-specific and essential roles of CBP/p300 in regulating adipose plasticity. *J. Endocrinol.* 240, 257–269

54. Mutlu, B., and Puigserver, P. (2021) GCN5 acetyltransferase in cellular energetic and metabolic processes. *Biochim. Biophys. Acta Gene Regul. Mech.* 1864, 194626

55. Yan, L., Jin, W., Zhao, Q., Cui, X., Shi, T., Xu, Y., Li, F., Jin, W., Zhang, Z., Zhang, Z., Tang, Q.-Q., and Pan, D. (2021) PWWP2B Fine-Tunes Adipose Thermogenesis by Stabilizing HDACs in a NuRD Subcomplex. *Adv. Sci. Weinh. Baden-Wurtt. Ger.* 8, e2102060

56. Dovey, O. M., Foster, C. T., and Cowley, S. M. (2010) Histone deacetylase 1 (HDAC1), but not HDAC2, controls embryonic stem cell differentiation. *Proc. Natl. Acad. Sci.* 107, 8242–8247

57. Artsi, H., Gurt, I., El-Haj, M., Müller, R., Kuhn, G. A., Ben Shalom, G., Cohen-Kfir, E., Abramowitz, E., Kandel, L., Safran, O., and Dresner-Pollak, R. (2019) Sirt1 Promotes a Thermogenic Gene Program in Bone Marrow Adipocytes: From Mice to (Wo)Men. *Front. Endocrinol.* 10, 126

58. Yao, L., Cui, X., Chen, Q., Yang, X., Fang, F., Zhang, J., Liu, G., Jin, W., and Chang, Y. (2017) Cold-Inducible SIRT6 Regulates Thermogenesis of Brown and Beige Fat. *Cell Rep.* 20, 641–654

59. Sambeat, A., Gulyaeva, O., Dempersmier, J., and Sul, H. S. (2017) Epigenetic Regulation of the Thermogenic Adipose Program. *Trends Endocrinol. Metab. TEM* 28, 19–31

60. Wang, Y., Gao, M., Zhu, F., Li, X., Yang, Y., Yan, Q., Jia, L., Xie, L., and Chen, Z. (2020) METTL3 is essential for postnatal development of brown adipose tissue and energy expenditure in mice. *Nat. Commun.* 11, 1648

61. Chen, L., Zhang, J., Zou, Y., Wang, F., Li, J., Sun, F., Luo, X., Zhang, M., Guo, Y., Yu, Q., Yang, P., Zhou, Q., Chen, Z., Zhang, H., Gong, Q., Zhao, J., Eizirik, D. L., Zhou, Z., Xiong, F., Zhang, S., and Wang, C.-Y. (2021) Kdm2a deficiency in macrophages enhances thermogenesis to protect mice against HFD-induced obesity by enhancing H3K36me2 at the Pparg locus. *Cell Death Differ.* 28, 1880–1899

62. Hoshii, T., Perlee, S., Kikuchi, S., Rahmutulla, B., Fukuyo, M., Masuda, T., Ohtsuki, S., Soga, T., Nabet, B., and Kaneda, A. (2022) SETD1A regulates transcriptional pause release of heme biosynthesis genes in leukemia. *Cell Rep.* 41, 111727

63. Zhao, Z., Yang, R., Li, M., Bao, M., Huo, D., Cao, J., and Speakman, J. R. (2022) Effects of ambient temperatures between 5 and 35 °C on energy balance, body mass and body composition in mice. *Mol. Metab.* 64, 101551

64. Chaffee, R. R., Clark, R. T., Reynafarje, B., Cunningham, M. D., and Bartlett, W. L. (1963) Some effects of cold-acclimation on the biochemistry and histology of the

hamster kidney. *Proc. Soc. Exp. Biol. Med. Soc. Exp. Biol. Med. N. Y. N* 113, 115–121

65. Yahata, T., and Kuroshima, A. (1989) Metabolic cold acclimation after repetitive intermittent cold exposure in rat. *Jpn. J. Physiol.* 39, 215–228

66. Klose, R. J., and Bird, A. P. (2006) Genomic DNA methylation: the mark and its mediators. *Trends Biochem. Sci.* 31, 89–97

67. Anastasiadi, D., Esteve-Codina, A., and Piferrer, F. (2018) Consistent inverse correlation between DNA methylation of the first intron and gene expression across tissues and species. *Epigenetics Chromatin* 11, 37

68. Neri, F., Rapelli, S., Krepelova, A., Incarnato, D., Parlato, C., Basile, G., Maldotti, M., Anselmi, F., and Oliviero, S. (2017) Intragenic DNA methylation prevents spurious transcription initiation. *Nature* 543, 72–77

69. Maunakea, A. K., Chepelev, I., Cui, K., and Zhao, K. (2013) Intragenic DNA methylation modulates alternative splicing by recruiting MeCP2 to promote exon recognition. *Cell Res.* 23, 1256–1269

70. The Consortium for Top Down Proteomics, Smith, L. M., and Kelleher, N. L. (2013) Proteoform: a single term describing protein complexity. *Nat. Methods* 10, 186–187

71. Young, N. L., DiMaggio, P. A., Plazas-Mayorca, M. D., Baliban, R. C., Floudas, C. A., and Garcia, B. A. (2009) High Throughput Characterization of Combinatorial Histone Codes. *Mol. Cell. Proteomics* 8, 2266–2284

72. Dang, X., Singh, A., Spetman, B. D., Nolan, K. D., Isaacs, J. S., Dennis, J. H., Dalton, S., Marshall, A. G., and Young, N. L. (2016) Label-Free Relative Quantitation of Isobaric and Isomeric Human Histone H2A and H2B Variants by Fourier Transform Ion Cyclotron Resonance Top-Down MS/MS. *J. Proteome Res.* 15, 3196–3203

73. Taylor, B. C., and Young, N. L. (2021) Combinations of histone post-translational modifications. *Biochem. J.* 478, 511–532

74. Kimura, H. (2013) Histone modifications for human epigenome analysis. *J. Hum. Genet.* 58, 439–445

75. Jain, K., Marunde, M. R., Burg, J. M., Gloor, S. L., Joseph, F. M., Poncha, K. F., Gillespie, Z. B., Rodriguez, K. L., Popova, I. K., Hall, N. W., Vaidya, A., Howard, S. A., Taylor, H. F., Mukhsinova, L., Onuoha, U. C., Patteson, E. F., Cooke, S. W., Taylor, B. C., Weinzapfel, E. N., Cheek, M. A., Meiners, M. J., Fox, G. C., Namitz, K. E. W., Cowles, M. W., Krajewski, K., Sun, Z.-W., Cosgrove, M. S., Young, N. L., Keogh, M.-C., and Strahl, B. D. (2023) An acetylation-mediated chromatin switch governs H3K4 methylation read-write capability. *eLife* 12, e82596

76. Hilfiker, A., Hilfiker-Kleiner, D., Pannuti, A., and Lucchesi, J. C. (1997) mof, a putative acetyl transferase gene related to the Tip60 and MOZ human genes and to the SAS genes of yeast, is required for dosage compensation in Drosophila. *EMBO J.* 16, 2054–2060

77. Suka, N., Luo, K., and Grunstein, M. (2002) Sir2p and Sas2p opposingly regulate acetylation of yeast histone H4 lysine16 and spreading of heterochromatin. *Nat. Genet.* 32, 378–383

78. Tovy, A., Reyes, J. M., Zhang, L., Huang, Y.-H., Rosas, C., Daquinag, A. C., Guzman, A., Ramabadran, R., Chen, C.-W., Gu, T., Gupta, S., Ortinau, L., Park, D., Cox, A. R., Rau, R. E., Hartig, S. M., Kolonin, M. G., and Goodell, M. A. (2022) Constitutive loss of DNMT3A causes morbid obesity through misregulation of adipogenesis. *eLife* 11, e72359

79. Wang, S., Cao, Q., Cui, X., Jing, J., Li, F., Shi, H., Xue, B., and Shi, H. (2021) Dnmt3b Deficiency in Myf5+-Brown Fat Precursor Cells Promotes Obesity in Female Mice. *Biomolecules* 11, 1087

80. Kim, A. Y., Park, Y. J., Pan, X., Shin, K. C., Kwak, S.-H., Bassas, A. F., Sallam, R. M., Park, K. S., Alfadda, A. A., Xu, A., and Kim, J. B. (2015) Obesity-induced DNA hypermethylation of the adiponectin gene mediates insulin resistance. *Nat. Commun.* 6, 7585

81. Qiao, L., Yoo, H. sun, Bosco, C., Lee, B., Feng, G.-S., Schaack, J., Chi, N.-W., and Shao, J. (2014) Adiponectin reduces thermogenesis by inhibiting brown adipose tissue activation in mice. *Diabetologia* 57, 1027–1036

82. Shin, K. C., Huh, J. Y., Ji, Y., Han, J. S., Han, S. M., Park, J., Nahmgoong, H., Lee, W. T., Jeon, Y. G., Kim, B., Park, C., Kang, H., Choe, S. S., and Kim, J. B. (2022) VLDL-VLDLR axis facilitates brown fat thermogenesis through replenishment of lipid fuels and PPARβ/δ activation. *Cell Rep.* 41, 111806

83. Carroll, J., Shannon, R. J., Fearnley, I. M., Walker, J. E., and Hirst, J. (2002) Definition of the nuclear encoded protein composition of bovine heart mitochondrial complex I. Identification of two new subunits. *J. Biol. Chem.* 277, 50311–50317

84. Goudriaan, J. R., Espirito Santo, S. M. S., Voshol, P. J., Teusink, B., van Dijk, K. W., van Vlijmen, B. J. M., Romijn, J. A., Havekes, L. M., and Rensen, P. C. N. (2004) The VLDL receptor plays a major role in chylomicron metabolism by enhancing LPL-mediated triglyceride hydrolysis. *J. Lipid Res.* 45, 1475–1481

85. Lorincz, M. C., Dickerson, D. R., Schmitt, M., and Groudine, M. (2004) Intragenic DNA methylation alters chromatin structure and elongation efficiency in mammalian cells. *Nat. Struct. Mol. Biol.* 11, 1068–1075

86. Vernia, S., Edwards, Y. J., Han, M. S., Cavanagh-Kyros, J., Barrett, T., Kim, J. K., and Davis, R. J. (2016) An alternative splicing program promotes adipose tissue thermogenesis. *eLife* 5, e17672

87. Chao, Y., Jiang, Y., Zhong, M., Wei, K., Hu, C., Qin, Y., Zuo, Y., Yang, L., Shen, Z., and Zou, C. (2021) Regulatory roles and mechanisms of alternative RNA splicing in adipogenesis and human metabolic health. *Cell Biosci.* 11, 66

88. Zhang, P., Wu, W., Ma, C., Du, C., Huang, Y., Xu, H., Li, C., Cheng, X., Hao, R., and Xu, Y. (2022) RNA-Binding Proteins in the Regulation of Adipogenesis and Adipose Function. *Cells* 11, 2357

89. Fuks, F., Hurd, P. J., Wolf, D., Nan, X., Bird, A. P., and Kouzarides, T. (2003) The methyl-CpG-binding protein MeCP2 links DNA methylation to histone methylation. *J. Biol. Chem.* 278, 4035–4040

90. Fujita, N., Watanabe, S., Ichimura, T., Tsuruzoe, S., Shinkai, Y., Tachibana, M., Chiba, T., and Nakao, M. (2003) Methyl-CpG binding domain 1 (MBD1) interacts with the Suv39h1-HP1 heterochromatic complex for DNA methylation-based transcriptional repression. *J. Biol. Chem.* 278, 24132–24138

91. Espada, J., Ballestar, E., Fraga, M. F., Villar-Garea, A., Juarranz, A., Stockert, J. C., Robertson, K. D., Fuks, F., and Esteller, M. (2004) Human DNA methyltransferase 1 is required for maintenance of the histone H3 modification pattern. *J. Biol. Chem.* 279, 37175–37184

92. Gu, H., Smith, Z. D., Bock, C., Boyle, P., Gnirke, A., and Meissner, A. (2011) Preparation of reduced representation bisulfite sequencing libraries for genome-scale DNA methylation profiling. *Nat. Protoc.* 6, 468–481

93. Huang, Y., Pastor, W. A., Shen, Y., Tahiliani, M., Liu, D. R., and Rao, A. (2010) The behaviour of 5-hydroxymethylcytosine in bisulfite sequencing. *PloS One* 5, e8888

94. Jin, S.-G., Kadam, S., and Pfeifer, G. P. (2010) Examination of the specificity of DNA methylation profiling techniques towards 5-methylcytosine and 5-hydroxymethylcytosine. *Nucleic Acids Res.* 38, e125

95. Pandeswari, P. B., and Sabareesh, V. (2019) Middle-down approach: a choice to sequence and characterize proteins/proteomes by mass spectrometry. *RSC Adv.* 9, 313–344

96. Patrie, S. M. (2016) in *Modern Proteomics – Sample Preparation, Analysis and Practical Applications*, Advances in Experimental Medicine and Biology., eds Mirzaei H, Carrasco M (Springer International Publishing, Cham), pp 171–200.

97. Moradian, A., Kalli, A., Sweredoski, M. J., and Hess, S. (2014) The top-down, middle-down, and bottom-up mass spectrometry approaches for characterization of

histone variants and their post-translational modifications. *PROTEOMICS* 14, 489–497

98. Tvardovskiy, A., Wrzesinski, K., Sidoli, S., Fey, S. J., Rogowska-Wrzesinska, A., and Jensen, O. N. (2015) Top-down and Middle-down Protein Analysis Reveals that Intact and Clipped Human Histones Differ in Post-translational Modification Patterns. *Mol. Cell. Proteomics* 14, 3142–3153

99. Han, X., Jin, M., Breuker, K., and McLafferty, F. W. (2006) Extending Top-Down Mass Spectrometry to Proteins with Masses Greater Than 200 Kilodaltons. *Science* 314, 109–112

100. Tran, J. C., Zamdborg, L., Ahlf, D. R., Lee, J. E., Catherman, A. D., Durbin, K. R., Tipton, J. D., Vellaichamy, A., Kellie, J. F., Li, M., Wu, C., Sweet, S. M. M., Early, B. P., Siuti, N., LeDuc, R. D., Compton, P. D., Thomas, P. M., and Kelleher, N. L. (2011) Mapping intact protein isoforms in discovery mode using top-down proteomics. *Nature* 480, 254–258

101. Plazas-Mayorca, M. D., Bloom, J. S., Zeissler, U., Leroy, G., Young, N. L., DiMaggio, P. A., Krugylak, L., Schneider, R., and Garcia, B. A. (2010) Quantitative proteomics reveals direct and indirect alterations in the histone code following methyltransferase knockdown. *Mol. Biosyst.* 6, 1719–1729

102. Vaquero, A., Scher, M., Erdjument-Bromage, H., Tempst, P., Serrano, L., and Reinberg, D. (2007) SIRT1 regulates the histone methyl-transferase SUV39H1 during heterochromatin formation. *Nature* 450, 440–444

103. Aebersold, R., Agar, J. N., Amster, I. J., Baker, M. S., Bertozzi, C. R., Boja, E. S., Costello, C. E., Cravatt, B. F., Fenselau, C., Garcia, B. A., Ge, Y., Gunawardena, J., Hendrickson, R. C., Hergenrother, P. J., Huber, C. G., Ivanov, A. R., Jensen, O. N., Jewett, M. C., Kelleher, N. L., Kiessling, L. L., Krogan, N. J., Larsen, M. R., Loo, J. A., Ogorzalek Loo, R. R., Lundberg, E., MacCoss, M. J., Mallick, P., Mootha, V. K., Mrksich, M., Muir, T. W., Patrie, S. M., Pesavento, J. J., Pitteri, S. J., Rodriguez, H., Saghatelian, A., Sandoval, W., Schlüter, H., Sechi, S., Slavoff, S. A., Smith, L. M., Snyder, M. P., Thomas, P. M., Uhlén, M., Van Eyk, J. E., Vidal, M., Walt, D. R., White, F. M., Williams, E. R., Wohlschlager, T., Wysocki, V. H., Yates, N. A., Young, N. L., and Zhang, B. (2018) How many human proteoforms are there? *Nat. Chem. Biol.* 14, 206–214

104. Young, N. L., DiMaggio, P. A., and Garcia, B. A. (2010) The significance, development and progress of high-throughput combinatorial histone code analysis. *Cell. Mol. Life Sci.* 67, 3983–4000

105. Bannister, A. J., Zegerman, P., Partridge, J. F., Miska, E. A., Thomas, J. O., Allshire, R. C., and Kouzarides, T. (2001) Selective recognition of methylated lysine 9 on histone H3 by the HP1 chromo domain. *Nature* 410, 120–124

106. Morris, S. A., Shibata, Y., Noma, K., Tsukamoto, Y., Warren, E., Temple, B., Grewal, S. I. S., and Strahl, B. D. (2005) Histone H3 K36 Methylation Is Associated with Transcription Elongation in *Schizosaccharomyces pombe*. *Eukaryot. Cell* 4, 1446–1454

107. Boros, J., Arnoult, N., Stroobant, V., Collet, J.-F., and Decottignies, A. (2014) Polycomb Repressive Complex 2 and H3K27me3 Cooperate with H3K9 Methylation To Maintain Heterochromatin Protein 1 at Chromatin. *Mol. Cell. Biol.* 34, 3662–3674

108. Schotta, G., Lachner, M., Sarma, K., Ebert, A., Sengupta, R., Reuter, G., Reinberg, D., and Jenuwein, T. (2004) A silencing pathway to induce H3-K9 and H4-K20 trimethylation at constitutive heterochromatin. *Genes Dev.* 18, 1251–1262

109. Wang, Z., Zang, C., Rosenfeld, J. A., Schones, D. E., Barski, A., Cuddapah, S., Cui, K., Roh, T.-Y., Peng, W., Zhang, M. Q., and Zhao, K. (2008) Combinatorial patterns of histone acetylations and methylations in the human genome. *Nat. Genet.* 40, 897–903

110. Iizuka, K., Bruick, R. K., Liang, G., Horton, J. D., and Uyeda, K. (2004) Deficiency of carbohydrate response element-binding protein (ChREBP) reduces lipogenesis as well as glycolysis. *Proc. Natl. Acad. Sci. U. S. A.* 101, 7281–7286

111. Izzo, L. T., Trefely, S., Demetriadou, C., Drummond, J. M., Mizukami, T., Kuprasertkul, N., Farria, A. T., Nguyen, P. T. T., Murali, N., Reich, L., Kantner, D. S., Shaffer, J., Affronti, H., Carrer, A., Andrews, A., Capell, B. C., Snyder, N. W., and Wellen, K. E. (2023) Acetylcarnitine shuttling links mitochondrial metabolism to histone acetylation and lipogenesis. *Sci. Adv.* 9, eadf0115

112. Hsu, J., Fatuzzo, N., Weng, N., Michno, W., Dong, W., Kienle, M., Dai, Y., Pasca, A., Abu-Remaileh, M., Rasgon, N., Bigio, B., Nasca, C., and Khosla, C. (2023) Carnitine octanoyltransferase is important for the assimilation of exogenous acetyl-L-carnitine into acetyl-CoA in mammalian cells. *J. Biol. Chem.* 299, 102848

113. Adamkova, K., Yi, Y.-J., Petr, J., Zalmanova, T., Hoskova, K., Jelinkova, P., Moravec, J., Kralickova, M., Sutovsky, M., Sutovsky, P., and Nevoral, J. (2017) SIRT1-dependent modulation of methylation and acetylation of histone H3 on lysine 9 (H3K9) in the zygotic pronuclei improves porcine embryo development. *J. Anim. Sci. Biotechnol.* 8, 83

114. Kodani, N., and Nakae, J. (2020) Tissue-Specific Metabolic Regulation of FOXO-Binding Protein: FOXO Does Not Act Alone. *Cells* 9, 702

115. Zhang, P., Tu, B., Wang, H., Cao, Z., Tang, M., Zhang, C., Gu, B., Li, Z., Wang, L., Yang, Y., Zhao, Y., Wang, H., Luo, J., Deng, C.-X., Gao, B., Roeder, R. G., and Zhu, W.-G. (2014) Tumor suppressor p53 cooperates with SIRT6 to regulate

gluconeogenesis by promoting FoxO1 nuclear exclusion. *Proc. Natl. Acad. Sci.* 111, 10684–10689

116. Meng, F., Qian, M., Peng, B., Peng, L., Wang, X., Zheng, K., Liu, Z., Tang, X., Zhang, S., Sun, S., Cao, X., Pang, Q., Zhao, B., Ma, W., Songyang, Z., Xu, B., Zhu, W.-G., Xu, X., and Liu, B. (2020) Synergy between SIRT1 and SIRT6 helps recognize DNA breaks and potentiates the DNA damage response and repair in humans and mice. *eLife* 9, e55828

117. Xiong, S., Salazar, G., Patrushev, N., and Alexander, R. W. (2011) FoxO1 Mediates an Autofeedback Loop Regulating SIRT1 Expression. *J. Biol. Chem.* 286, 5289–5299

118. Kuang, J., Chen, L., Tang, Q., Zhang, J., Li, Y., and He, J. (2018) The Role of Sirt6 in Obesity and Diabetes. *Front. Physiol.* 9, 135

119. Rifaï, K., Judes, G., Idrissou, M., Daures, M., Bignon, Y.-J., Penault-Llorca, F., and Bernard-Gallon, D. (2018) SIRT1-dependent epigenetic regulation of H3 and H4 histone acetylation in human breast cancer. *Oncotarget* 9, 30661–30678

120. Nic-Can, G. I., Rodas-Junco, B. A., Carrillo-Cocom, L. M., Zepeda-Pedreguera, A., Peñaloza-Cuevas, R., Aguilar-Ayala, F. J., and Rojas-Herrera, R. A. (2019) Epigenetic Regulation of Adipogenic Differentiation by Histone Lysine Demethylation. *Int. J. Mol. Sci.* 20, 3918

121. Nakae, J., Cao, Y., Hakuno, F., Takemori, H., Kawano, Y., Sekioka, R., Abe, T., Kiyonari, H., Tanaka, T., Sakai, J., Takahashi, S.-I., and Itoh, H. (2012) Novel repressor regulates insulin sensitivity through interaction with Foxo1. *EMBO J.* 31, 2275–2295

Tables

***Table 1**. Online HPLC parameters for histones H4 and H3.* 1 µL of sample was injected per run after resuspension to a standard concentration (200 ng/µL for H4; 2 µg/µL for H3). The same buffers were used with different gradients (See Linear Gradient section). Histone species were introduced to the Orbitrap Fusion Lumos mass spectrometer using nano-electrospray ionization as they eluted.

	Histone H4	Histone H3
Sample Volume	1 µL	1 µL
Temperature	4.0 [°C]	4.0 [°C]
Buffer A	2% ACN 0.1% FA	2% ACN 0.1% FA
Buffer B	98% ACN 0.1% FA	98% ACN 0.1% FA
Equilibration	Duration = 5.000 [min]	Duration = 5.000 [min]
Column	10 cm x 100 µm self-packed C3	10 cm x 100 µm self-packed C3
Flow Rate	0.200 [µL/min]	0.200 [µL/min]

Linear Gradient	Time (minutes)	% Buffer B	Time (minutes)	% Buffer B
	0	29.0 [%]	0	4.0 [%]
	0.5	29.0 [%]	0.5	4.0 [%]
	70	35.0 [%]	70	15.0 [%]
	75	98.0 [%]	105	35.0 [%]
	80	98.0 [%]	110	98.0 [%]
	85	5.0 [%]	115	98.0 [%]
			120	5.0 [%]

Mouse BAT Cold Stress

Table 2. *Expression of epigenetic modifiers, one-carbon metabolic genes, and alternative splicing factors is altered in response to chronic thermogenic activation as measured by RNA-seq.* TN: thermoneutral; RT: room temperature; SC: severe cold.

	SC vs TN		SC vs RT		RT vs TN		
Gene	**Log_2FC**	**P_{adj}**	**Log_2FC**	**P_{adj}**	**Log_2FC**	**P_{adj}**	**Category**
Dnmt1	-0.40	7.02E-03	0.28	8.49E-02	-0.73	1.33E-06	DNA Methyltransferase
Dnmt3a	-0.38	1.53E-03	0.04	0.77	-0.47	1.16E-04	DNA Methyltransferase
Dnmt3b	-1.30	2.18E-06	-	-	-0.75	6.45E-03	DNA Methyltransferase
Acly	3.69	5.10E-11	1.03	1.19E-02	2.62	2.92E-05	Acetyl-CoA Generation
Acss2	2.52	2.64E-33	-0.08	0.77	2.56	1.36E-28	Acetyl-CoA Generation
Crat	1.14	1.15E-35	0.27	9.10E-05	0.82	6.26E-16	Acetyl-CoA Generation
Crot	0.43	6.96E-04	0.09	0.44	0.30	1.82E-02	Acetyl-CoA Generation
Smyd4	1.32	3.28E-16	1.06	6.11E-13	0.21	0.32	Histone Modification
Fcor	1.23	3.40E-25	-0.79	2.18E-15	1.98	3.80E-98	Histone Modification
Sirt5	0.94	4.31E-09	0.00	0.98	0.91	1.59E-06	Histone Modification
Kdm5c	0.65	1.12E-12	0.24	5.52E-03	0.36	1.02E-04	Histone Modification
N6amt1	0.62	5.38E-07	0.05	0.75	0.52	8.27E-05	Histone Modification
H1f0	0.51	1.15E-04	0.16	0.27	0.31	1.68E-02	Histone Modification
Setd7	0.50	2.28E-03	0.50	3.85E-04	-0.03	0.90	Histone Modification
Kdm3a	0.50	8.89E-03	0.55	1.69E-02	-0.09	0.69	Histone Modification
Kdm8	0.50	1.06E-02	0.20	0.54	0.27	0.42	Histone Modification
Hdac2	0.46	4.84E-06	0.12	0.35	0.30	2.12E-02	Histone Modification
Setd3	0.41	1.23E-06	-0.05	0.68	0.42	2.77E-05	Histone Modification
Kat2b	0.37	4.19E-03	0.15	0.28	0.18	0.20	Histone Modification
Prmt7	0.24	2.90E-02	0.16	0.16	0.03	0.84	Histone Modification
Kdm2b	0.13	0.43	0.54	5.61E-03	-0.45	3.21E-02	Histone Modification
Hdac5	-0.07	0.50	-0.30	2.30E-04	0.19	2.87E-02	Histone Modification
Hdac3	-0.16	0.08	-0.47	3.87E-10	0.27	1.68E-03	Histone Modification
Hdac10	-0.24	4.81E-02	-0.28	3.87E-02	0.00	1.00	Histone Modification
Kdm5b	-0.33	1.26E-02	-0.31	1.74E-02	-0.06	0.68	Histone Modification
Hat1	-0.38	1.32E-03	-0.26	3.02E-02	-0.16	0.22	Histone Modification
Chaf1a	-0.53	3.24E-02	-	-	-1.07	1.34E-04	Histone Modification
Smyd3	-0.56	3.30E-03	-0.48	1.85E-02	-0.12	0.52	Histone Modification
Hdac7	-0.64	9.63E-11	-0.09	0.54	-0.60	1.62E-07	Histone Modification
Suv39h1	-1.08	3.18E-08	-0.35	0.16	-0.77	3.52E-04	Histone Modification
Hdac9	-1.20	1.16E-06	-	-	-0.94	2.93E-05	Histone Modification
Slc25a32	1.47	3.61E-13	0.72	7.85E-03	0.71	1.54E-02	One-Carbon Metabolism
Sfxn1	1.14	5.20E-18	-0.07	0.59	1.17	1.37E-19	One-Carbon Metabolism
Mthfd2l	0.95	4.60E-15	-0.05	0.72	0.96	1.00E-15	One-Carbon Metabolism

Mouse BAT Cold Stress

Aldh1l1	0.91	1.88E-10	-0.12	0.59	0.99	2.07E-07	One-Carbon Metabolism
Tcn2	0.72	1.82E-16	0.06	0.63	0.61	1.32E-09	One-Carbon Metabolism
Mthfd2	0.68	1.64E-03	1.31	5.77E-12	-0.67	1.24E-02	One-Carbon Metabolism
Sardh	0.64	5.69E-10	0.00	0.99	0.60	5.28E-04	One-Carbon Metabolism
Chdh	0.60	4.24E-06	0.12	0.31	0.44	1.76E-03	One-Carbon Metabolism
Pemt	0.54	2.33E-03	-0.32	0.13	0.82	4.06E-05	One-Carbon Metabolism
Slc19a1	0.52	7.30E-04	-0.24	0.26	0.72	1.50E-04	One-Carbon Metabolism
Ahcyl1	0.46	2.56E-03	0.12	0.24	0.30	0.07	One-Carbon Metabolism
Fpgs	-0.30	0.07	0.24	0.22	-0.58	2.12E-03	One-Carbon Metabolism
Shmt2	-0.31	4.47E-03	-0.13	0.23	-0.22	0.08	One-Carbon Metabolism
Sfxn3	-0.52	2.24E-02	0.40	3.60E-02	-0.96	3.48E-05	One-Carbon Metabolism
Mat2a	-0.68	5.56E-08	-0.08	0.75	-0.64	1.58E-03	One-Carbon Metabolism
Mtr	-0.86	7.19E-24	-0.30	8.94E-03	-0.61	2.98E-09	One-Carbon Metabolism
Shmt1	-1.01	1.80E-14	-0.71	3.35E-09	-0.34	2.32E-02	One-Carbon Metabolism
Aldh1l2	-1.36	9.27E-06	-	-	-1.18	1.31E-04	One-Carbon Metabolism
Igf2bp2	0.79	3.92E-03	0.93	3.03E-07	-0.20	0.60	Alternative Splicing
Elavl1	0.44	1.02E-04	0.23	1.37E-02	0.17	0.15	Alternative Splicing
Ybx3	0.11	0.37	-0.19	0.10	0.25	3.62E-02	Alternative Splicing
Ybx1	-0.08	0.34	-0.39	3.03E-05	0.27	6.71E-03	Alternative Splicing
Ctcf	-0.13	0.12	0.01	0.90	-0.19	4.19E-02	Alternative Splicing
Srsf1	-0.33	6.75E-04	-0.32	3.91E-03	-0.05	0.68	Alternative Splicing
Srsf2	-0.33	4.43E-04	-0.20	0.15	-0.18	0.18	Alternative Splicing
Srsf11	-0.40	5.36E-04	-0.52	9.59E-10	0.08	0.49	Alternative Splicing
Rbm4	-0.45	0.14	-0.58	3.30E-02	0.10	0.76	Alternative Splicing
Srsf5	-0.59	1.70E-06	-0.48	3.81E-04	-0.16	0.10	Alternative Splicing
Srsf3	-0.62	2.17E-07	-0.27	6.08E-02	-0.39	4.10E-03	Alternative Splicing
Srsf7	-0.66	4.31E-11	-0.09	0.50	-0.61	3.03E-06	Alternative Splicing
Nova2	-0.78	2.15E-05	0.04	0.87	-0.86	1.46E-06	Alternative Splicing
Pspc1	-0.80	8.13E-04	-0.52	3.80E-02	-0.32	0.30	Alternative Splicing

Table 3. *Integration of RRBS data with RNA-seq reveals genes that may be regulated by altered DNA methylation in response to different housing temperatures.* DMPs: differentially methylated promoters; DEGs: differentially expressed genes; TN: thermoneutral; RT: room temperature; SC: severe cold.

	SC vs TN				**RT vs TN**			
	DMPs		**DEGs**		**DMPs**		**DEGs**	
Gene Name	**Meth Diff**	**P_{adj}**	**Fold Change**	**P_{adj}**	**Meth Diff**	**P_{adj}**	**Fold Change**	**P_{adj}**
Tspan31	-36.93	1.53E-47	1.20	1.06E-02				
Dnajc14	-34.23	1.67E-28	1.28	1.83E-06				
Car13	-31.99	8.74E-42	2.25	7.28E-19	-30.66	4.79E-38	1.53	1.24E-07
Gm33699	-25.58	4.08E-34	6.57	2.73E-13				
Lyplal1	-16.43	9.92E-10	2.65	2.59E-28	-19.18	4.58E-17	1.78	1.43E-06
Uba1	-15.99	4.05E-23	1.25	7.21E-04				
Dlg3	-11.02	1.55E-29	1.29	8.61E-03				
Vma21	-6.75	4.50E-14	1.80	1.48E-14	-6.03	1.68E-11	1.53	2.66E-08
Vldlr	-6.28	2.40E-08	1.38	5.22E-03	-6.86	9.66E-14	1.78	1.06E-06
Ndufb11	-5.19	1.47E-17	1.15	3.60E-02	-5.39	3.89E-23	1.62	3.75E-08
Car8					-5.28	3.30E-03	1.60	7.67E-04
Tpcn2					14.30	8.34E-05	0.54	2.90E-03

Figures

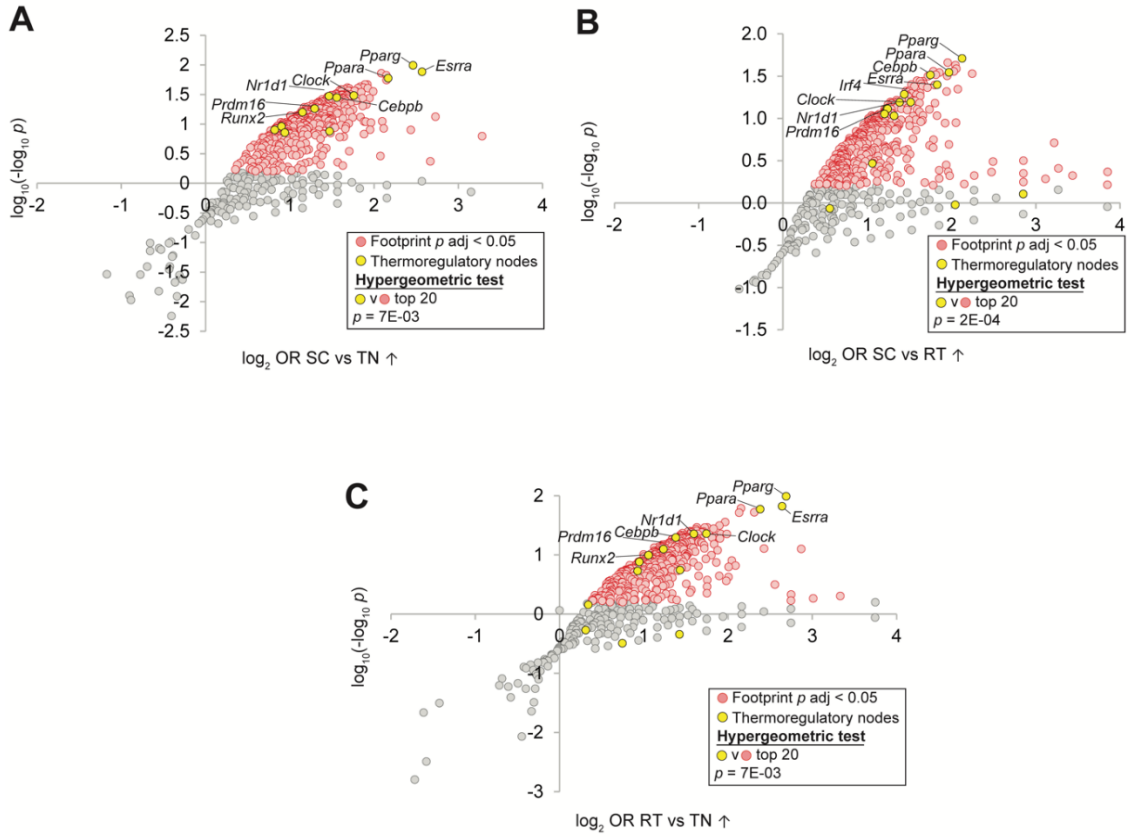

D

Class	Family	Symbol	SC vs TN ↑	SC vs TN ↓	SC vs RT ↑	SC vs RT ↓	RT vs TN ↑	RT vs TN ↓
Acetyltransferases	CBP/p300	*Crebbp*	E-60		E-40		E-30	
		Ep300	E-30	E-30	E-40			E-30
	Chromodomain Y like	*Cdyl*		E-20				E-20
	Lysine acetyltransferases (KAT)	*Kat2a*	E-30		E-20		E-20	
		Kat5	E-20		E-20		E-20	
		Kat8	E-30		E-20		E-30	
	Nuclear receptor coactivator (NCOA)	*Ncoa2*	E-30		E-20		E-30	
Deacetylases	Histone deacetylases (HDAC)	*Hdac1*	E-30		E-20		E-30	
		Hdac2	E-30		E-20		E-30	
		Hdac3	E-30	E-20	E-30	E-20	E-30	E-20
	Sirtuins (SIRT)	*Sirt1*		E-20				E-20
		Sirt6	E-20		E-20			
Methyltransferases	ASH like methyltransferase	*Ash2l*	E-40		E-20		E-30	
	Euchromatic histone-lysine N-methyltransferases	*Ehmt2*		E-20				
	Histone-lysine N-methyltransferases (KMT)	*Kmt2a*	E-30		E-20	E-20	E-30	E-20
		Kmt2b	E-40		E-20		E-30	
		Kmt2c	E-20	E-30	E-30	E-20	E-20	E-30
		Kmt2d	E-30		E-20	E-20	E-30	
	Methyltransferase-like (METTL)	*Mettl3*	E-30		E-20		E-30	
	SET domain-containing (SETD)	*Setd1a*	E-40		E-20		E-40	
		Setdb1	E-20	E-20	E-20		E-20	
Demethylases	Histone-H3-lysine demethylases (KDM)	*Kdm1a*	E-30		E-30	E-20	E-30	
		Kdm2a	E-20		E-20		E-20	
		Kdm2b	E-20	E-30	E-20	E-20		E-30
		Kdm4a		E-20				
		Kdm4c	E-30		E-20		E-30	
		Kdm5a	E-30		E-20		E-30	
		Kdm6a	E-30		E-20		E-30	
		Kdm6b	E-30	E-20	E-20	E-20	E-30	
	Jumonji domain containing	*Jmjd6*	E-20		E-20		E-20	E-20

p <
E-60
E-50
E-40
E-30
E-20
E-10
E-5
NS

Figure 1. *High confidence transcriptional target (HCT) intersection analysis resolves epigenetic writer transcriptional footprints in cold challenge-regulated gene sets.* In panels a-c, nodes that have the strongest (higher odds ratio, OR) and most significant (lower *p*-value) footprints within the indicated cold challenge-induced gene set are distributed towards the upper right of the plot. Scatterplot showing enrichment of nodes with established roles in thermal regulation among nodes that have the most significant intersections with **(a)** SC vs TN-induced genes; **(b)** SC vs RT-induced genes; and **(c)** RT vs TN-induced genes. **(d)** HCT intersection *p*-values for selected epigenetic writers within cold challenge-induced genes are indicated in the form of a heatmap. HCT intersection analysis was carried out as described in the Methods section. White cells represent $p > 0.05$ intersections. The intensity of the color scheme is proportional to the confidence of the intersection between HCTs for a particular node and genes induced (red, ↑) or repressed (blue, ↓) in each cold challenge contrast. Lower confidence (higher *p*) intersections are towards the yellow end of the spectrum and higher confidence (lower *p*) intersections are towards the brick red end of the spectrum. Full numerical data are in Supplemental File 1. TN: thermoneutral; RT: room temperature; SC: severe cold.

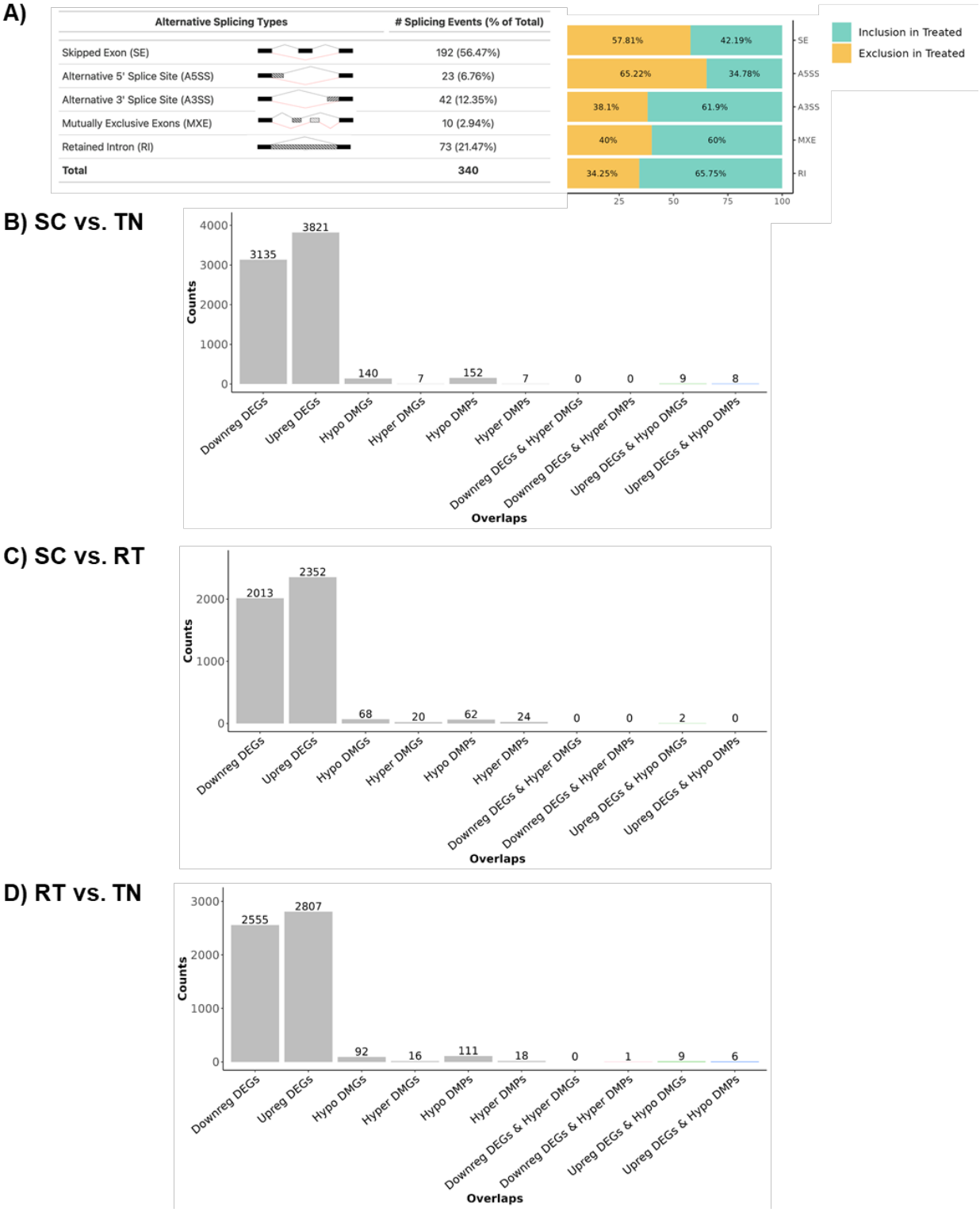

Figure 2. *Alternative splice variants and reduced representation bisulfite sequencing (RRBS) data reveal changes in brown adipose tissue associated with housing temperature.* **(a)** A

comparison of SC vs TN housing RNA-seq data reveals differential expression of alternate splice variants in BAT. Integrated RNA-seq and RRBS data for **(b)** SC vs TN housed mice. **(c)** SC vs RT housed mice; and **(d)** RT vs TN housed mice. RRBS data shown are for n=4 per group with percent methylation difference > |5|, $p_{adj} < 0.05$. DEG: differentially expressed genes. DMP: differentially methylated promoters. DMG: differentially methylated genes. TN: thermoneutral; RT: room temperature; SC: severe cold.

Mouse BAT Cold Stress

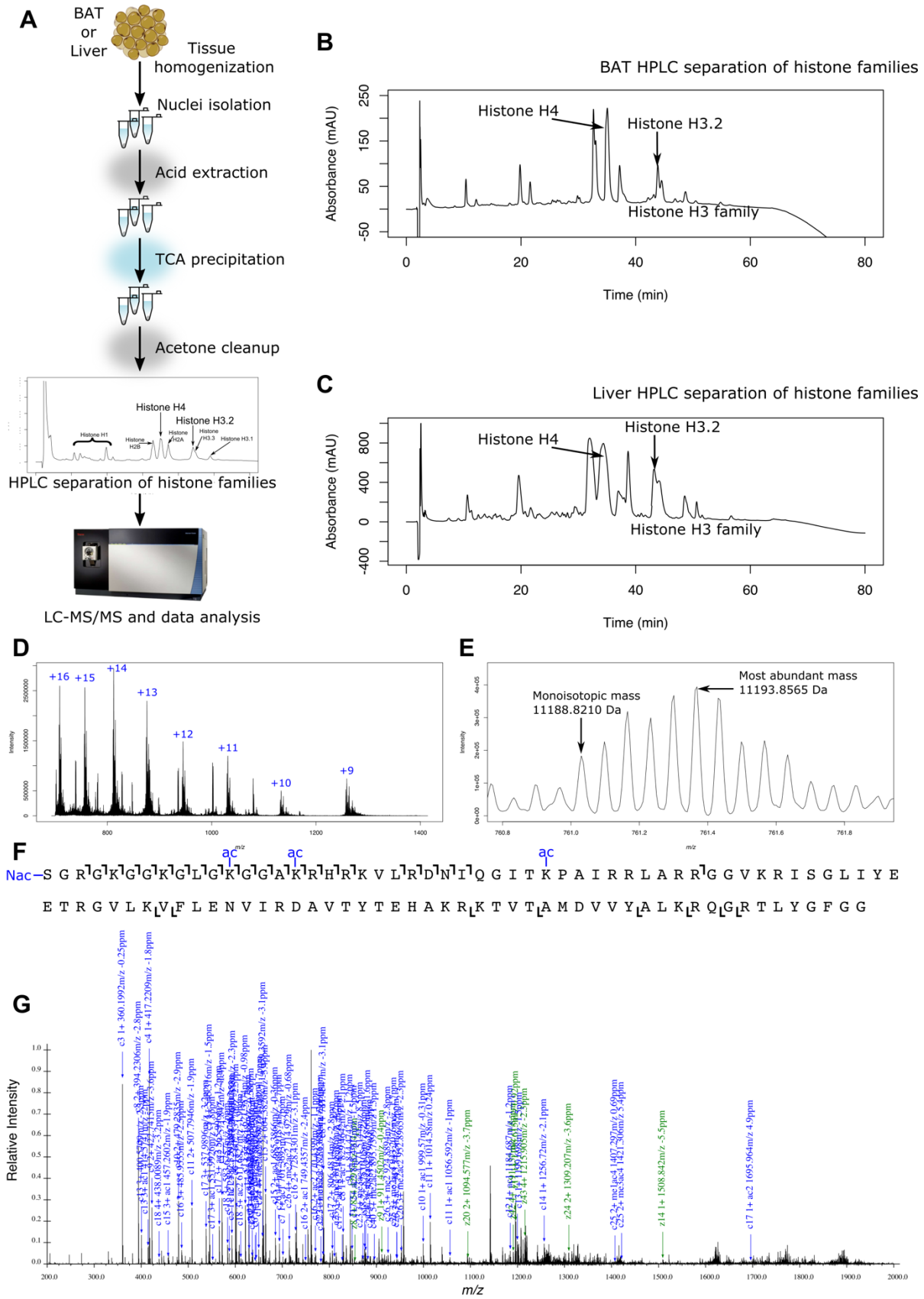

Figure 3. *Workflow to obtain histone proteoform data from brown adipose tissue and liver.* **(a)** The general workflow includes tissue homogenization, nuclei isolation, acid extraction, HPLC separation of histone families, and LC-MS/MS data acquisition. HPLC separation of histones shows a clean separation of histone families and H3 variants for **(b)** BAT and **(c)** liver. **(d)** MS1 average spectra of histone H4 extracted from BAT from 40 to 80 minutes show clear +16 to +9 charge states matching the *m/z* of histone H4. **(e)** The MS1 spectrum of 11,193.8565 Da species (761.2961 *m/z*, charge +15) matches a mass of H4 with N-terminal acetylation + 0 methylations + 3 acetylations + 0 phosphorylations with less than 10 ppm error. **(f)** The ion map from MS2 fragmentation of species from (e) shows unambiguous localization information for the proteoform H4 <N-acK12acK16acK31ac> from a mass change at less than 10 ppm error. **(g)** Annotated MS2 spectrum shows most abundant peaks are from the same proteoform, <N-acK12acK16acK31ac>, with less than 10 ppm error. Together, these methods enable the absolute quantitation of BAT and liver histone proteoforms.

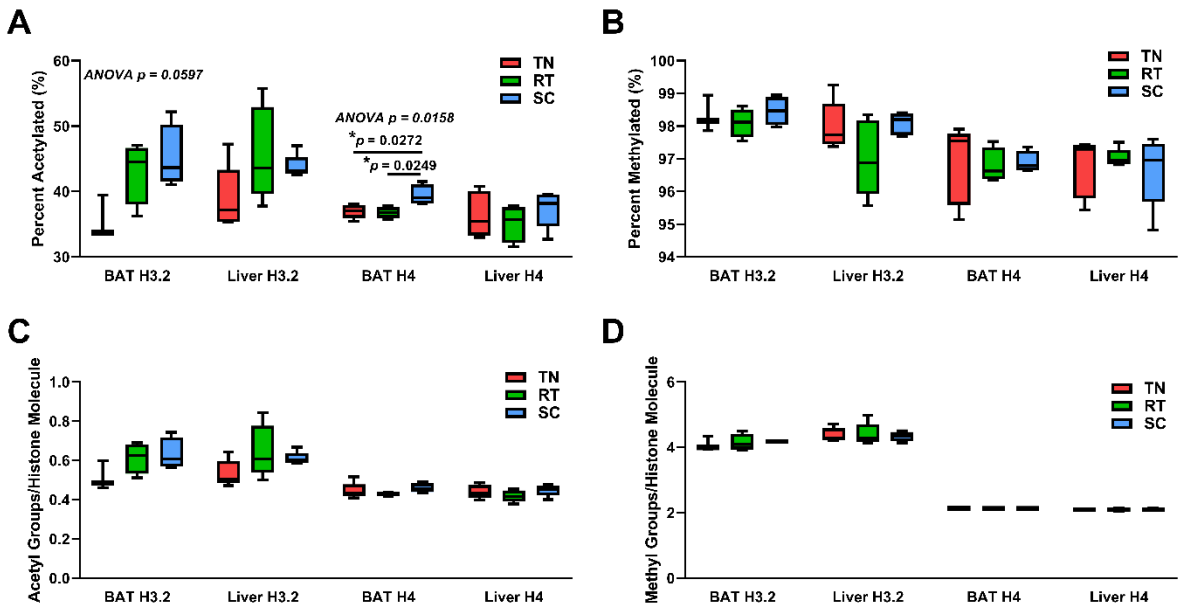

Figure 4. *Housing temperature alters bulk histone acetylation, but not methylation, in BAT and has no effect on bulk histone acetylation or methylation in liver.* Percent **(a)** acetylated (1+ acetylation) and **(b)** methylated (1+ methylation) histones H3.2 and H4 isolated from liver and BAT. Number of **(c)** acetyl groups and **(d)** methyl groups (K4me2 = 2 methyl groups) per histones H3.2 and H4 isolated from liver and BAT. One-way ANOVA testing was conducted for all histone data from each tissue comparing TN, RT, and SC housing conditions, and *p*-values are indicated in each plot. TN: thermoneutral; RT: room temperature; SC: severe cold.

Mouse BAT Cold Stress

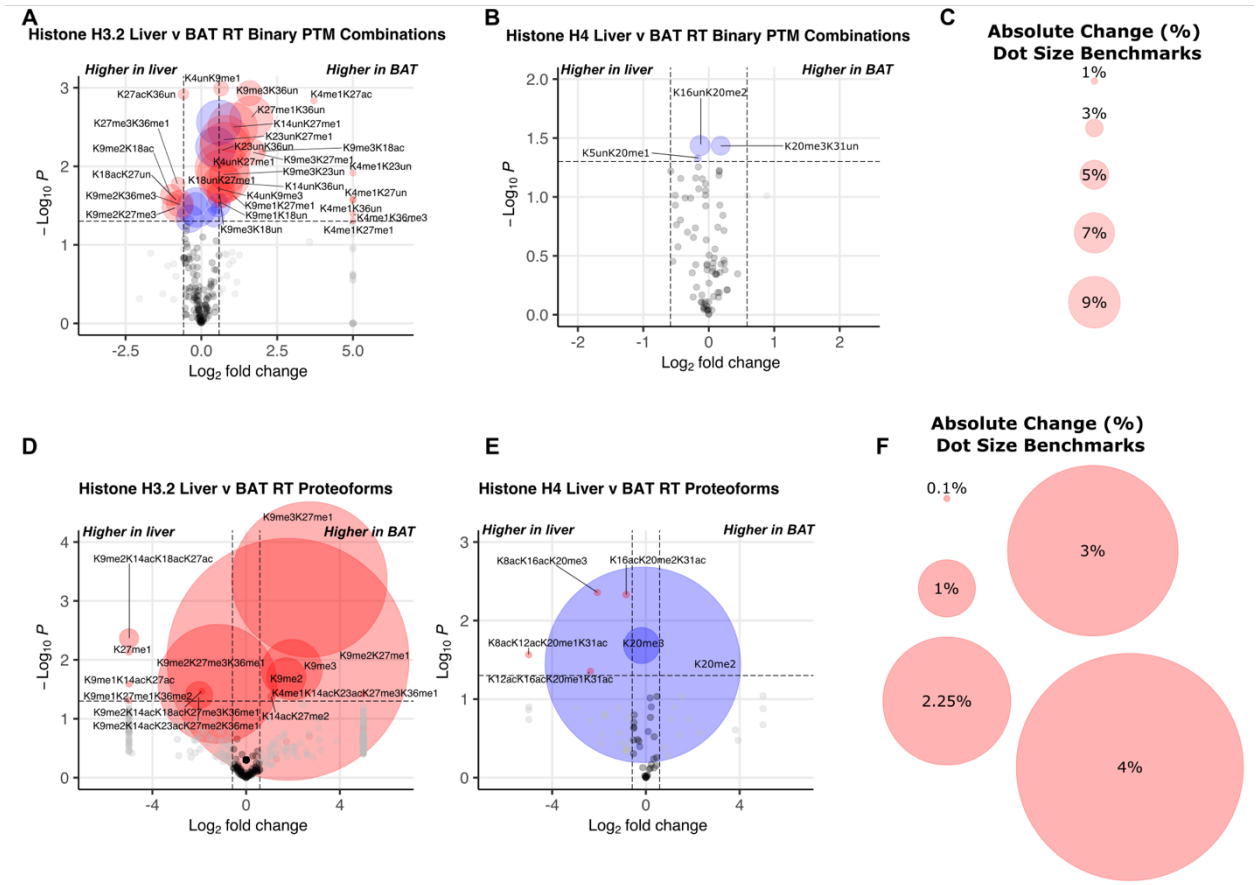

Figure 5. *BAT and liver are epigenetically different at room temperature.* **(a)** Histone H3.2 and **(b)** histone H4 binary PTM combinations in BAT and liver. **(c)** Dot size references for binary volcano plots (*a,b*). **(d)** Histone H3.2 and **(e)** histone H4 proteoforms from BAT and liver. **(f)** Dot size references for proteoform volcano plots (d.e). P-values were calculated using Welch's t-test. Volcano plots show cutoffs of 1.5 for fold change and $p < 0.05$. RT: room temperature.

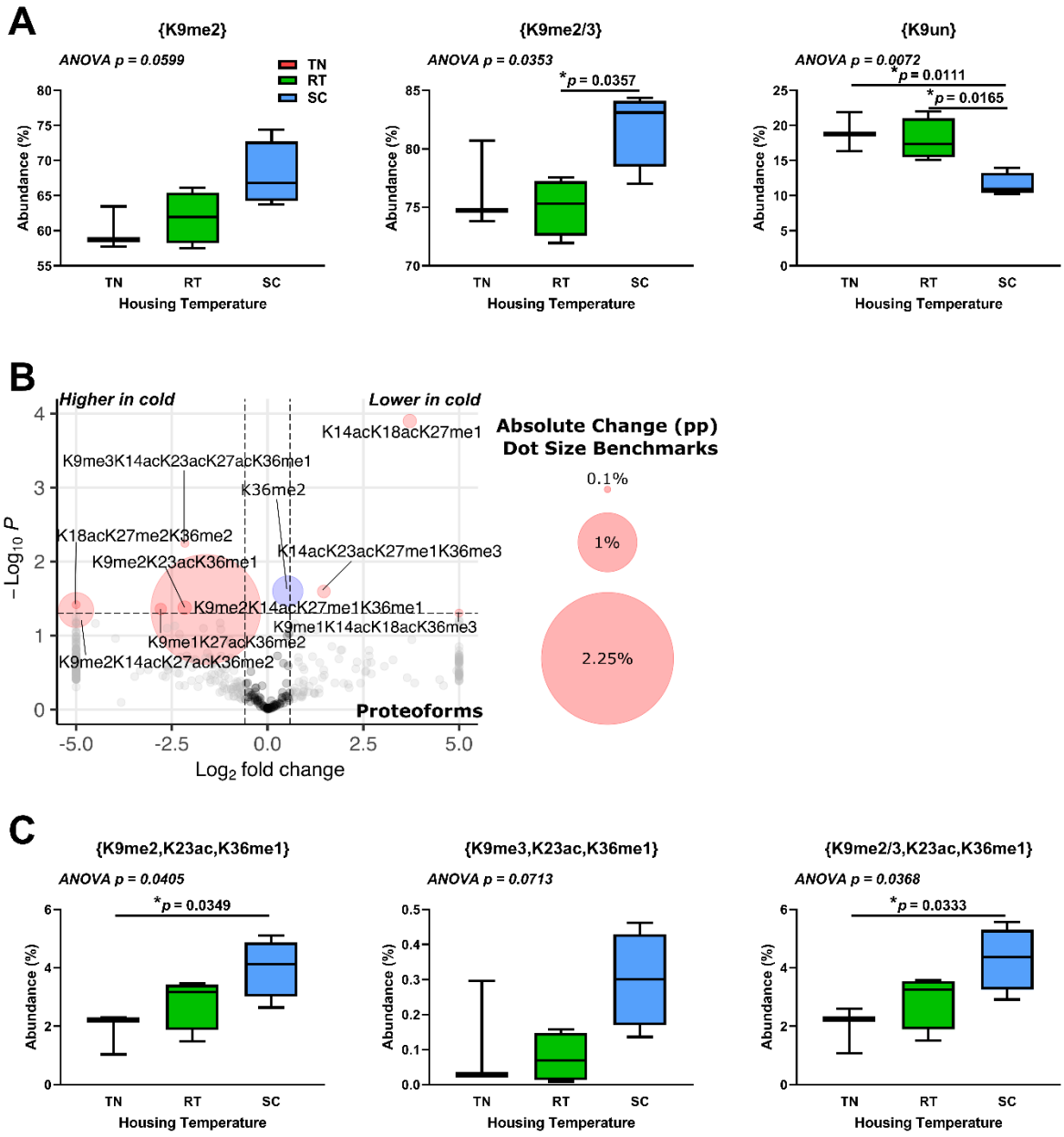

Figure 6. *Housing temperature significantly alters histone H3.2 K9me2- or K9me3-containing proteoforms in brown adipose tissue.* **(a)** Selected discrete H3.2 PTM abundance at different housing temperatures. **(b)** Proteoform changes between SC and TN. Dot size corresponds to absolute percentage point change. **(c)** Ternary (3-PTM) combinations show significant differences with K9 di- and tri-methylation, K23 acetylation,

and K36 monomethylation. Welch's t-test was used for volcano plot data, with cutoffs of 1.5 for fold change and $p < 0.05$. One-way ANOVA testing was conducted for all PTM data comparing TN, RT, and SC housing conditions, and *p*-values are indicated in each plot. TN: thermoneutral; RT: room temperature; SC: severe cold.

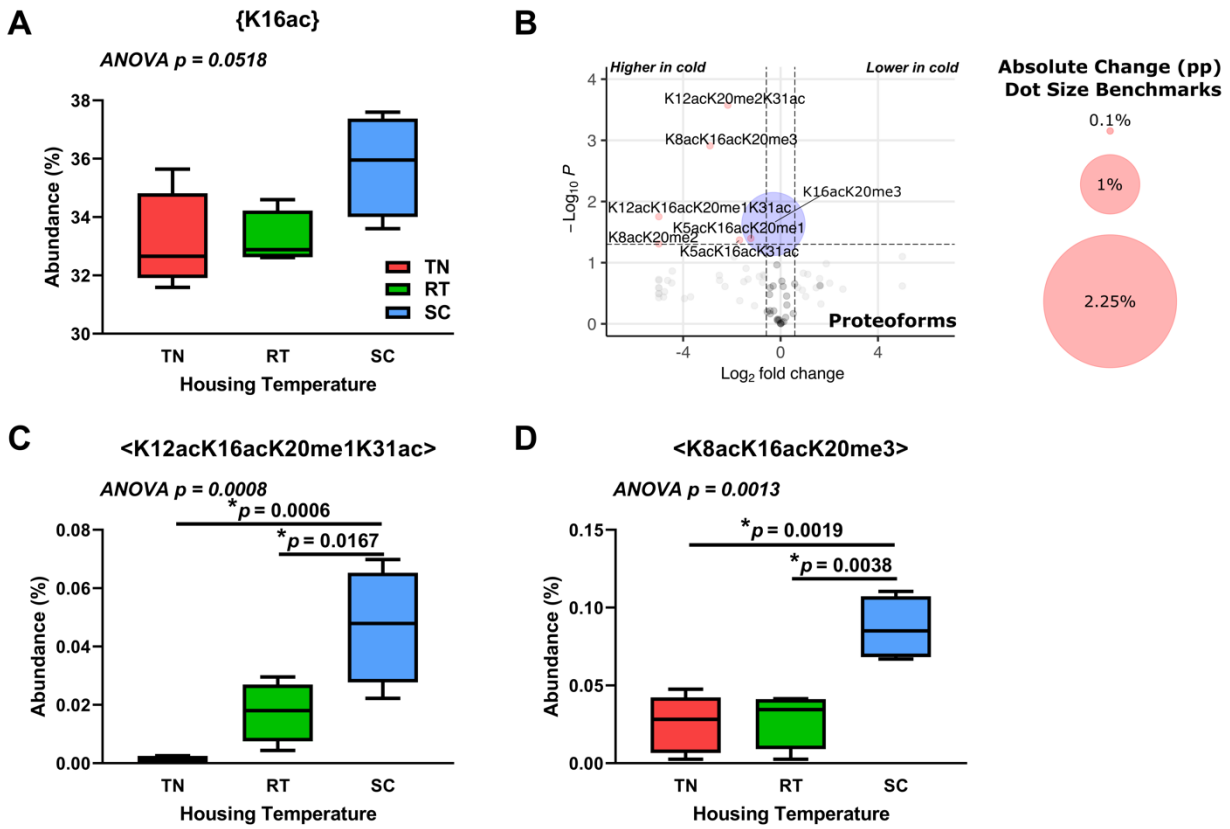

Figure 7. *Housing temperature significantly alters histone H4 K16ac-containing proteoforms in brown adipose tissue.* **(a)** Discrete K16ac PTM marks on histone H4 at different housing temperatures. **(b)** Histone H4 proteoforms from BAT from SC vs TN housing temperatures. Dot size corresponds to absolute percentage point change. **(c)** H4<K12acK16acK20me1K31ac> proteoform abundance at different housing temperatures. **(d)** H4<K8acK16acK20me3> proteoform abundance at different housing temperatures. Welch's t-test was used for volcano plot data, with cutoffs of 1.5 for fold change and $p < 0.05$. One-way ANOVA testing was conducted for all data comparing TN, RT, and SC housing conditions, and *p*-values are indicated in each plot. TN: thermoneutral; RT: room temperature; SC: severe cold.